6-16-2016 12:00 AM

The Development Of Novel Imaging Modalities & High-throughput Drug Screening Platforms In The Drosophila Melanogaster Model of Human Calcium Oxalate Nephrolithiasis

Sohrab Naushad Ali
The University of Western Ontario

Supervisor
Dr. Hassan Razvi
The University of Western Ontario Joint Supervisor
Dr. Hon Sing Leong
The University of Western Ontario

Graduate Program in Surgery
A thesis submitted in partial fulfillment of the requirements for the degree in Master of Science
© Sohrab Naushad Ali 2016

Follow this and additional works at: https://ir.lib.uwo.ca/etd

Part of the Disease Modeling Commons

Recommended Citation

Abstract

Nephrolithiasis is a common urological disorder. Despite advances in the surgical treatment of kidney stone disease, research into its prevention and medical management remain stagnant. This is due to lack of viable pre-clinical models to study the disorder. In this project, we develop and characterize a robust *Drosophila melanogaster* model for human calcium oxalate nephrolithiasis. Using this model, we have developed intravital imaging techniques to study stone formation and novel high-throughput drug screening platforms. We successfully demonstrate calcium oxalate stone formation by sodium oxalate and ethylene glycol supplementation, with subsequent intravital imaging using bisphosphonate based fluorescent probes. Screening of 360 experimental compounds has revealed 6 compounds that inhibit calcium oxalate stone formation. We intend to further investigate the mechanism of action of these compounds, use them as a starting point for rational drug design and to develop *Drosophila melanogaster* models for other kidney stone types.

Keywords

Acknowledgments

I would like to thank the *University of Western Ontario* and the faculty at the Department of Surgery for allowing me to be part of this excellent graduate program. The opportunity to conduct research at the Leong Lab has been a life changing experience for me.

I wish to extend my sincerest gratitude to my supervisors Dr. Hassan Razvi and Dr. Hon Sing Leong. Dr. Razvi, you have always been an inspiration to me and I am honored to have had the opportunity to work with you. The lessons I have learnt during my time with you have been invaluable in my development as an academic urologist. Thank you for accepting me as a student and for encouraging me every step of the way. I look forward to working with you in the future and advancing urological research in new and exciting ways. Hon, you have been a tremendous force in my life over the past two years and I am extremely lucky to have had you as supervisor, a mentor and a friend. You have taught me everything I know about being an academician and clinician scientist. Thank you for having me as part of your laboratory and for teaching me what it takes to succeed. I will always be in your debt.

I would like to thank Dr. Jeremy Burton for being part of my supervisory committee, plus his support and input throughout my project. I wish to thank all the faculty members at the Department of Surgery including Dr. John Denstedt and Dr. Nicholas Power for their continuous support, Dr. Abdel-Rahman Lawendy for his guidance and Janice Sutherland for always being there to answer my questions.

I would also like to thank all the members of the Leong Lab that made working here such a memorable experience. Especially Yohan, Sabine, Dajung, Dr. Khurram Siddiqi, Carson,

Karla and Rachel. Thank you for enduring with me through those long hours at the lab.

Lastly, I would like to thank my father Dr. Mian Naushad Ali and my mother Dr. Shazia Sadaf for always believing in me. I could not be where I am today without their love, help and support.

Table of Contents

List of Tables

List of Figures

List of Appendices

Chapter 1

1 Introduction

Nephrolithiasis is a common urological disorder with an estimated prevalence of 8.4% in North America[1]. Studies such as the one conducted by the National Health and Nutrition Examination Survey (NHANES) reveal that the prevalence is steadily rising, from a modest 3.8% reported in 1976 to 8.4% in 2010[2]. It is estimated that 19% of men and 9% of women will develop a symptomatic stone during their lifetime[1]. Although mortality rates due to stone disease are low, the morbidity is significant and is exacerbated by stone recurrence, with rates as high as 50% in the first five years and 80% throughout life[3]. Kidney stone disease also continues to be a significant healthcare burden. The total spending on nephrolithiasis related healthcare is estimated at a staggering US$ 5.3 billion annually, with 3.1 million work days lost, that account for an additional indirect cost of US$ 775 million annually[4,5].

1.1 Kidney Stone Subtypes

The vast majority of kidney stones are calcium based and account for 75% of all stones formed[6]. Of these, 80% are calcium oxalate and the rest are calcium phosphate[7]. Although some stones are pure, most are heterogeneous in composition, which reflect the complex pathophysiological pathways that govern stone formation. Most calcium oxalate stones also contain small quantities of hydroxyapatite and uric acid[6,8]. Uric acid stones are the second most common, accounting for 8-14% of stones formed. 5% of these are

pure uric acid and others contain small amounts of hydroxyapatite and struvite[6]. The third most common is the bacterial infection associated struvite (magnesium ammonium phosphate) stone at 2-6%[9]. The purely genetic cystine stone accounts for the remainder 2-3%[10]. Xanthine, an additional genetic stone subtype, is extremely rare and makes up only 0.1% of total stone burden[11]. Occasionally, high doses of drugs such as triamterene, sulphonamides and indinavir can precipitate and form crystals in the urinary tract[12].

The distribution of various stone types in a typical North American population are illustrated in **Figure 1**.
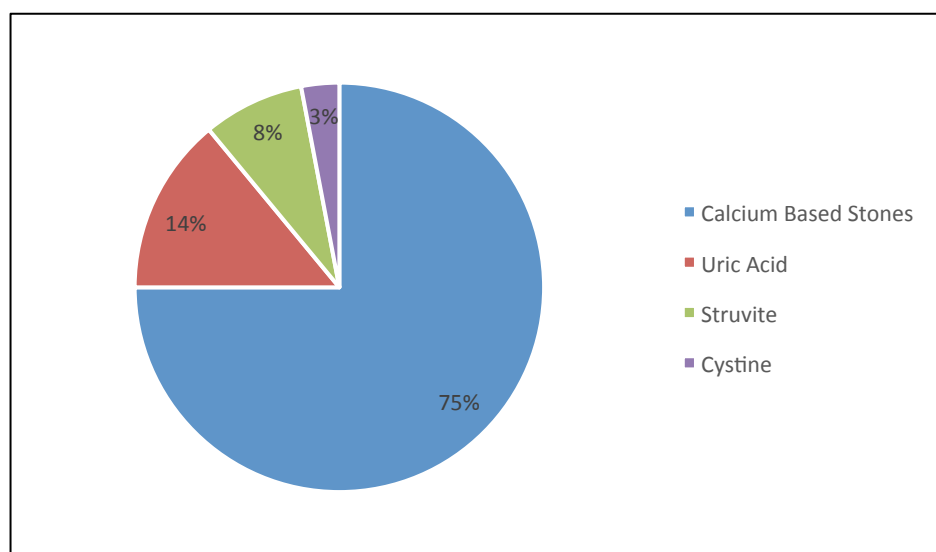
Figure 1: Distribution of stone subtypes in a North American population.

1.2 Pathogenesis of Kidney Stone Disease

The pathogenesis of kidney stone disease is complex and often poorly understood. It encompasses a wide variety of genetic and metabolic imbalances such as hypercalciuria and hyperoxaluria plus environmental factors such as the diet that collectively regulate

urine composition[13]. Generally, the underlying defect in all stone types is the dysregulation of urinary composition and pH that allows for the super saturation and precipitation of its constituents[6]. Other common risk factors include urinary stasis due to obstruction, low fluid intake that results in a concentrated urine and dietary trends such as an increased consumption of salt and protein[6,7,9]. Subtle factors such as climate, temperature changes and geographic location have also been implicated in the rising prevalence of kidney stone disease[14,15].

1.2.1   Calcium Oxalate

Calcium oxalate nephrolithiasis is a complex genetic disorder that is characterized by multiple metabolic abnormalities and environmental factors such as the diet[16,17].

Hypercalciuria (a urinary calcium excretion of > 6.24 mmol/day in women and > 7.49 mmol/day in men) is the most common metabolic abnormality identified in 30-60% of calcium stone formers[18,19]. Two thirds of these patients present with 'idiopathic' hypercalciuria and have no identifiable cause. Idiopathic hypercalciuria can either be due to increased intestinal absorption (absorptive), increased bone turnover (resorptive) or increased renal losses (renal hypercalciuria), with most patients exhibiting more than one abnormality. The pathophysiology of absorptive hypercalciuria is varied, with some patients exhibiting signs of vitamin D dependent hypercalciuria characterized by increased circulating levels of activated vitamin D, that causes increased intestinal absorption of calcium and increased bone resorption through osteoclast activation[20–22]. A subgroup of hypercalciuric patients have vitamin D independent hypercalciuria, which is most likely due to an up regulation of the vitamin D receptor (VDR), as shown in a

variety of animal studies[23,24]. Renal leak hypercalciuria is less common and caused by defective tubular reabsorption of filtered calcium which leads to increased parathyroid hormone release, increased activated vitamin D and increased intestinal calcium absorption[25]. Chronic acidemia, such as that which occurs in renal tubular acidosis, also increases the risk of calcium oxalate stone formation by causing hypercalciuria, hypocitriuria and an acidic urine[26]. The most common form of resorptive hypercalciuria is primary hyperparathyroidism, which leads to increased levels of parathyroid hormone causing increased bone turnover and increased intestinal calcium absorption[16,27]. Hypophosphatemia has also been implicated in the development of hypercalciuria by stimulating the activation of vitamin D[28]. Mutations in the sodium-hydrogen exchange regulator factor 1 (*NHERF1*) have been identified in several patients as a possible cause for renal phosphate leak leading to hypophosphatemia[29,30].

Hyperoxaluria (a urinary oxalate excretion of > 0.5 mmol/day) is detected in 10-50% patients and is an independent risk factor in calcium oxalate stone formation[31]. Endogenous oxalate overproduction occurs in inborn errors of metabolism such as primary hyperoxaluria or metabolic breakdown of excess dietary vitamin C[32–35]. Increased intestinal absorption of oxalate occurs in low calcium diets or due to increased intestinal calcium absorption, such as in hypercalciuric patients or small bowel disorders like Crohn's disease, surgical bowel resection and other malabsorption syndromes[36–38]. Normally, calcium in the gut forms complexes with oxalate to increase enteric clearance. A reduction of calcium in the gut leads to the increased absorption of oxalate and concomitant oxaluria[39,40]. Recently, the alteration of the gut microbiota with the loss of

Oxalobacter formigenes, an oxalate degrading bacteria, has also been implicated in increasing the risk of calcium oxalate stone formation[41–44].

Hyperuricosuria is also commonly detected in patients with calcium oxalate stones[45]. However, the link between high levels of uric acid and calcium stone formation has not yet been established[19]. Previous theories for uric acid crystals serving as a nidus for calcium oxalate deposition have since been refuted[6].

Other mechanisms by which calcium oxalate stones form are reductions in the levels of urinary crystallization inhibitors such as citrate and the endogenously produced tamm-horsfall protein (uromodulin), nephrocalcin and uropontin[46,47]. Citrate acts by forming soluble complexes with calcium to increase renal clearance and prevent binding to oxalate[48]. Citrate also inhibits crystal aggregation, an important step in stone formation[49]. Hypocitriuria (a urinary citrate of < 1.67 mmol/day) is associated with an increased risk of calcium stone formation and can occur in isolation or with other metabolic abnormalities. Hypocitriuria is common in acidemic states such as chronic diarrhea, renal tubular acidosis and certain drugs. Diets high in protein also result in lower levels of urinary citrate[50,51].

Diet also plays an important role in the formation of calcium oxalate stones by regulating the urinary composition. Low fluid intake leads to concentration of the urine and super saturation of calcium and oxalate. By far, the most effective intervention for reducing the risk of stones is increasing fluid intake[52]. Alcohol and sugar sweetened drinks are associated with increased risk of stone formation, while orange and lemon juice that are rich in citrate, plus tea and coffee reduce the risk of stone formation[53–56]. Diets high in

sodium and animal protein increase the risk of stone formation[50,57]. Diets high in potassium and phytates seem to lower risk[58,59].

1.2.2   Uric Acid

Uric acid, which is a byproduct of normal purine metabolism, has two dissociable protons and generally exists as hydrogen urate that forms soluble salts with sodium, potassium and ammonium[60]. The two main pathological features that predispose a patient to uric acid stone formation are an acidic urinary pH and increased amounts of uric acid in the urine. Alterations in the urinary pH and a high concentration of uric acid drive the conversion of soluble hydrogen urate into the relatively less soluble uric acid.

$$H^+ + Urate \; \rightarrow Uric\,Acid$$
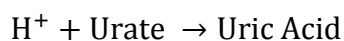
The effects of urinary pH on uric acid solubility are dramatic, with the solubility of dropping to 0.09 mmol/l at a pH of 5 compared to 1.2 mmol/l at a pH of 7[60–62]. The association between urinary pH and uric acid crystal precipitation explains the high prevalence of uric acid stones in patients that have a low fluid intake, chronic diarrhea or small bowel disease that cause a loss of bicarbonate and a concentrated acidic urine[13,36]. Uric acid stones are also more prevalent in populations that live in hot arid climates[63]. Recently, type 2 diabetes and metabolic syndrome have also been implicated in the increased risk of forming uric acid stones by reducing ammoniagenesis and reducing urinary pH[64,65]. Diets rich in red meat can increase the risk of forming uric acid stones by providing excesses of methionine which is metabolized to sulfuric acid, which in turn decreases the urinary pH[50].

Hyperuricosuria can also contribute to uric acid stone formation with extremely high urinary levels causing crystallization of uric acid regardless of the urinary pH[66]. This is common in patients with gout, myeloproliferative disorders, tumor lysis syndrome and other genetic enzyme defects such as *glucose-6-phosphatase* deficiency[67,68].

1.2.3 Struvite

Struvite is a hard mineral complex composed of magnesium ammonium phosphate[69]. It generally forms in alkaline conditions that cause a decrease in the solubility of phosphate which then forms complexes with other urinary constituents such as magnesium and ammonium. The underlying pathology of struvite stones are infection with urea splitting bacteria such as *Klebsiella*, *Proteus*, *Pseudomonas* and *Staphylococcus*[70,71]. These bacteria produce *Urease* which split urea into ammonia and carbon dioxide.

$$\text{Urea} \rightarrow 2NH_3 + CO_2$$
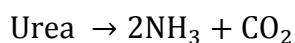
The ammonia combines with water to produce ammonium and a hydroxyl ion which increases urinary pH.

$$NH_3 + H_2O \rightarrow NH_4 + OH^-$$
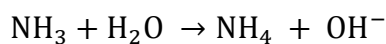
Struvite stones often grow very rapidly forming staghorn stones that cause the complete occlusion of the renal collecting system. Females and patients at higher risk of urinary tract infection commonly form struvite stones[72,73].

1.2.4   Cystine

Cystine, which is a homo-dimer of the amino acid cysteine, is a rare cause of kidney stone disease in humans. It is caused by the impaired proximal tubular reabsorption of filtered cystine due to mutations in the dibasic amino acid transporters *SLC3A1* and *SLC7A9*[10]. The cystine transporter belongs to a family of heteromeric amino acid transporters, with the *SLC3A1* gene coding for the heavy rBAT unit and the *SLC7A9* coding for the light $b^{0,+}AT$ unit[74]. Both genes are required for proper localization and transit of the transporter to the cell apical membrane. The defective transporters cause abnormalities in renal and intestinal cystine absorption leading to high concentrations of cystine in the urine with super saturation and crystallization[75,76]. Patients with cystine nephrolithiasis usually present at an early age and have a protracted disease history[77].

1.2.5   Miscellaneous

Xanthine nephrolithiasis, an extremely rare form of kidney stone disease, is caused by mutations of the enzyme *Xanthine dehydrogenase* that catalyzes the conversion of hypoxanthine to xanthine and xanthine to uric acid[11,78]. This leads to xanthinuria with super saturation and precipitation of xanthine crystals.

Routinely prescribed medications can, on occasion, cause crystal deposition and nephropathy. Drugs such as sulfadiazine for toxoplasmosis, acyclovir for herpes zoster and indinavir, a protease inhibitor for HIV infection, reach high concentrations in the renal tubules and due to their relative insolubility precipitate and form small stones[79].

1.3 Presentation of Kidney Stone Disease

Pain is the most common symptom associated with kidney stone disease, although a subset of patients have clinically asymptomatic nephrolithiasis and are diagnosed inadvertently during radiologic imaging of the abdomen for unrelated causes. Patients with asymptomatic nephrolithiasis that have not experienced an episode of renal colic in the past, are less likely of becoming symptomatic in the future[80]. However, the inverse is true in patients with a previous history of kidney stones that are diagnosed with asymptomatic nephrolithiasis.

The pain associated with kidney stones is usually colicky in nature and may wax and wane or present acutely as an unrelenting severe flank pain. Unilateral flank pain and costo-vertebral angle tenderness are common in stones that cause obstruction in the renal pelvis or upper ureter. Stones that cause obstruction in the lower ureter cause pain that radiates to the groin, testicle or labium. Patients with acute ureteric obstruction usually present with excruciating pain, accompanied by nausea and vomiting. Persistent vomiting can lead to metabolic alkalosis and electrolyte abnormalities.

Both gross and microscopic hematuria occur in approximately 70% of patients with nephrolithiasis, however, the absence of hematuria in a patient with flank pain does not rule out kidney stone disease[81–84]. The time of onset of acute pain seems to correlate positively with the presence of hematuria, with hematuria being present in 95% of patients at day one and in only 68% at day three[82].

Besides pain and hematuria, patients can present with passage of fine gravel or small stones. Persistent obstruction of the urinary tract can lead to kidney dysfunction and permanent damage. Occasionally, patients may also present with fever due to superimposed urinary tract infections caused by urinary stasis and obstruction. Kidney stones are known to harbor virulent bacteria and are thus a nidus for infection[85].

1.4 Current Animal Models for Human Nephrolithiasis

Despite being a significant healthcare burden and a risk factor for chronic renal disease, research into and our understanding of the mechanisms that govern stone formation remain limited. This is mostly due to the lack of suitable pre-clinical models that recapitulate the pathophysiology of the disorder. An ideal kidney stone disease model should be simple, highly reliable and consistent in stone formation, whilst maintaining fidelity to the elemental composition of human stones. Additionally, these models must also be amenable to non-invasive imaging and permit the investigator to antagonize stone formation in order to assess the value of potential therapeutic agents.

Historically, rats have been the animal of choice for studying nephrolithiasis, however, canine and porcine models also exist[86–89]. Although the kidneys of these animals have been used in the past for understanding renal structure and physiology, there are fundamental anatomical differences that make them poor candidates as models for kidney stone disease. Their kidneys are generally smaller in size, unipapillate compared to the multipapillate human kidneys and have fewer nephrons and tubules which make them incapable of forming large kidney stones[90]. Additionally, spontaneous nephrolithiasis in

rats is extremely rare and there are currently no reports of spontaneous stone formation in the urinary tracts of these animals[91].

Stone formation in the rat model of nephrolithiasis is induced by the administration of lithogenic agents such as sodium oxalate, ammonium oxalate, hydroxy-L-proline, ethylene glycol and glycolic acid, all of which produce hyperoxaluria[88,92–95]. Most of the lithogenic agents are administered either by supplementation in the diet or through intraperitoneal injections, which can prove cumbersome[86,93,94,96]. Additionally, the administration of these lithogenic agents does not accurately recreate the metabolic milieu required for stone formation and are often nephrotoxic leading to renal failure and death[91,97]. The size, amount and duration of calcium oxalate crystal excretion is directly related to the duration of lithogenic administration, with crystal formation ceasing after the lithogenic agent is withdrawn[98]. Most of the calcium oxalate crystals form in the tubular lumina and are non-adherent to the renal epithelium, subsequently being washed out in the urine[98].

Rat models of nephrolithiasis are also highly unreliable, with stone formation following unpredictable and protracted time lines. Low dose concentrations of 1% *w/v* ethylene glycol produced calcium oxalate nephrolithiasis in only 3 of 13 male Sprague-Dawley rats and 0 of 12 females at 4 weeks[99]. Combinations of lithogenic agents produced similar results. Rats administered a combined treatment of 0.75% *w/v* ethylene glycol and 2% *w/v* ammonium oxalate produced crystalluria at 3 days and nephrolithiasis at 7 days. These stones were generally < 200 μm in size and only found in the bladder aspirate[100–102]. Similar results were obtained in more recent studies using ethylene glycol and glyoxylate administration. Minimal crystal deposition was seen at 1 and 2 weeks in rats

fed a 1% *w/v* ethylene glycol diet, with intraperitoneal injections of glyoxylate slightly improving results[94].

In addition to the above drawbacks, the only method to accurately verify and monitor stone deposition, is to sacrifice the animals. This causes an unnecessary loss of animals and increased costs. Similarly, the use of this model does not allow the investigator to visualize stone burden *in vivo*, limiting their ability to identify therapeutic targets or evaluate the efficacy of a potential therapy. The infrastructure requirements and costs associated with rat based studies make large scale studies unfeasible. Small sample sizes used in most studies lead to questionable results at best. Also, the processing of the kidney tissue does not allow for the collection of stone material, which leads to difficulties in verifying stone composition.

Currently, the majority of rat models aim to elucidate the mechanisms involved in calcium oxalate stone formation. Although rat models exist for other stone types, such as cystine, these models suffer the same setbacks described above[103]. Further work is needed to refine the current animal models for human nephrolithiasis.

In light of the above limitations and the cost prohibitive nature of working with current animal models, the urological community has been prompted to develop newer, more novel models for human nephrolithiasis.

1.5　The *Drosophila melanogaster* Model of Human Nephrolithiasis

Drosophila melanogaster (DM) has recently emerged as a viable model for human nephrolithiasis[104]. Although it might seem like an unlikely candidate at first, it shares a lot in common with humans and has many advantages over current animal models.

1.5.1　Advantages of *Drosophila melanogaster*

Drosophila is a versatile model organism that has been studied for over a 100 years, with novel research carried out in the field of genetics, including translational research in human disorders[105]. It is a proven translational and drug discovery model for numerous conditions such as Alzheimer's disease and diabetes[106]. Furthermore, discoveries using *Drosophila* have improved our understanding of a variety of human renal diseases. For example, research in *Drosophila* identified the gene *vha55* that encodes for the B subunit of the V-ATPase pump, mutations of which lead to renal acidification and death[107,108]. This work preceded the discovery of sub-lethal mutations in human V-ATPase pumps as a cause for renal tubular acidosis[109]. Xanthinuria, a rare cause of nephrolithiasis, which is due to mutations in the enzyme *Xanthine dehydrogenase* (XHD), was unknown until the cloning of homologs in *Rosy* and *Maroon-like Drosophila*, leading to the discovery of mutations in the human molybdenum cofactor sulfurase gene[78]. Similarly, other genes such as *dPrestin*, which encodes for the transmembrane oxalate transporter SLC26A5 in *Drosophila*, have been implicated in the formation of calcium oxalate stones[110].

The *Drosophila* genome (180 million base pairs) is fully sequenced and highly conserved with humans. Despite millennia of divergent evolution, over 70% of DM genes have human homologs[111]. These homologs and other gene orthologs for human disorders can easily be identified using online tools such as the DIOPT-DIST database[112]. An exhaustive online database for all fly genes and microarray expression data are freely available to the research community[113,114]. Additionally, the fly genome is easily modifiable using established genetic tools such as the GAL4/UAS system[115]. This bi-partite system allows for simple mating based schemes that can spatio-temporally control the expression of the *Drosophila* genome. Through systematic mutagenesis and P-element insertion, hundreds of fly lines have been produced that contain upstream activation sequences (UAS) and the yeast transcription activator factor (GAL4)[116]. Two fly lines, one containing the UAS construct followed by the gene of interest and another expressing GAL4 in a tissue specific pattern, are mated to produce progeny that possess both. GAL4 binds to the UAS activating the downstream sequence resulting in either gene expression or knockdown through small hairpin RNA interference.

Drosophila has a short life cycle of 14 days and an adult life span of approximately 40-50 days, which allows for multiple experiments to be carried out in a short period of time. Various strains of DM are freely available and can be mail ordered within days, usually at minimal cost (~$20 CAD), through the international stocking centers at Bloomington, Indiana, USA, the National Institute of Genetics, Mishima, Japan or the Kyoto Stock Centre, Kyoto, Japan. The *Drosophila* research community is vibrant, with most researchers publically sharing their proprietary fly lines. These fly stocks can be maintained with minimal reagents and at minimal cost (<$20 CAD per year) which

makes their long term use feasible. Fly husbandry is an easy skill that can be learned with very little training and does not require an investment in expensive infrastructure.

Finally, current ethics guidelines exempt the use of invertebrates such as DM, which removes the ethical constraints associated with research in current animal models of human nephrolithiasis.

1.5.2   *Drosophila* Renal Anatomy

The DM renal system is composed of two components, the nephrocytes and the malpighian tubules. The nephrocytes are a distinct group of cells concentrated near the esophagus and heart. They filter the insect hemolymph, which bathe the internal organs, similar to the human glomerulus. These specialized cells are high adapted and are analogous to the podocytes in the human glomerulus **(Figure 2)**. The filtration function of human podocytes is highly dependent on the slit diaphragm component proteins such as *nephrin* and *NEPH1*. Orthologs of both these genes are high expressed in *Drosophila*, loss of which, results in a filtration syndrome similar to congenital nephrotic syndrome of the Finnish type[117].
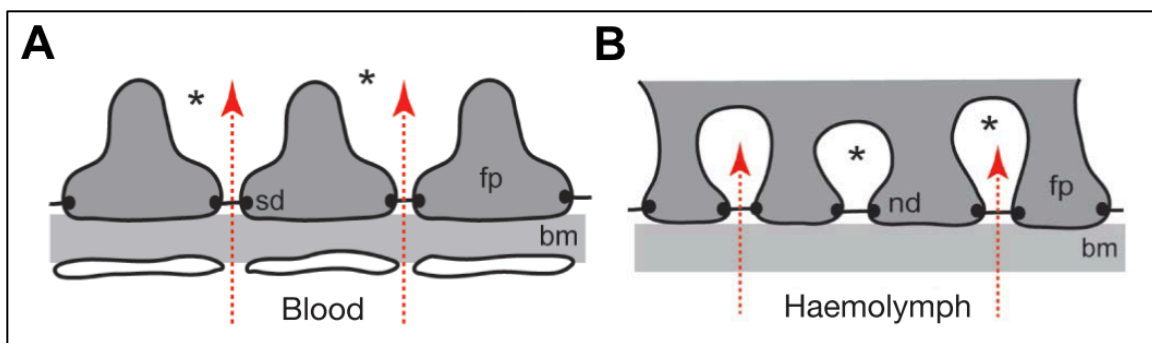
Figure 2: Schematic diagram comparing vertebrate podocytes to insect nephrocytes. (A) Podocyte glomerular filtration barrier with basement membrane (bm), slit diaphragm (sd) and foot processes (fp). Ultrafiltration direction is show with red arrows. (B) Insect nephrocytes with slit membranes similar to podocytes. Adapted with permission from Weavers H. *et. al* 2010.

DM have 4 malpighian tubules, which are divided into anterior and posterior pairs. These tubules dangle freely in the insect hemolymph and coalesce into a common ureter before draining into the gut at the junction between the mid and the hind gut **(Figure 3)**. Each tubule is approximately 2 mm long and has a 17 μm wide lumen[118]. The malpighian tubules are further divided into distinct segments. The initial segments are generally wider and serve as a storage organ for naturally formed concretions of calcium phosphate and glycosaminoglycans[119]. These concretions are thought to be involved in fly calcium homeostasis similar to the human skeleton. A short transitional segment is followed by a long main segment which is made up of principal cells with interspersed stellate cells that collectively take part in ion and solute transport analogous to the human nephron **(Figure 4)**.
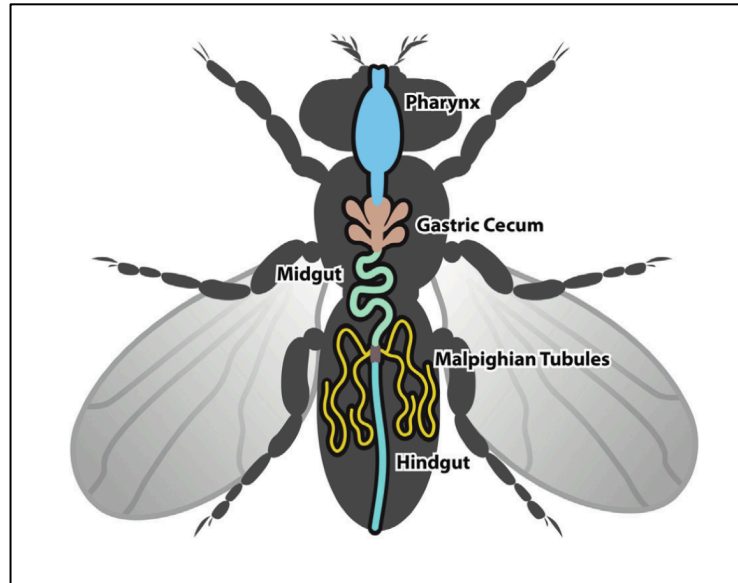
Figure 3: The *Drosophila melanogaster* excretory tract consists of 2 pairs of malpighian tubules, 1 anterior and 1 posterior, and are connected to the gut via a common ureter. Adapted with permission from Miller J. *et. al* 2013.
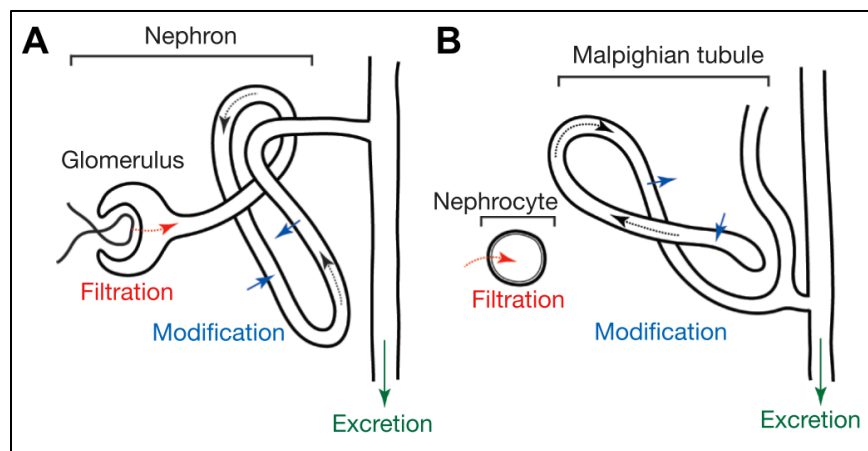
Figure 4: Similarities between the human renal nephron and *Drosophila* malpighian tubules. Adapted with permission from Weavers H. *et. al* 2010.

The main segment is mainly responsible for urine production, with the principal cells

possessing ion and solute transporters similar to the cells in the proximal convoluted

tubules and the collecting ducts in human kidneys **(Figure 5)**. The principal cells contain

basolateral membrane transporters for Na^+, K^+ and Cl^- plus an Na^+ dependent bicarbonate

exchanger. Ion gradients are maintained using an $H^+ATPase$ pump which drives the

secondary transport of Na^+ and K^+. The stellate cells mostly regulate H_2O and Cl^-

balance. Besides having a lot in common with the human nephron, *Drosophila*

malpighian tubules are easily dissected and visualized using simple techniques such

bright field and polarized light microscopy.
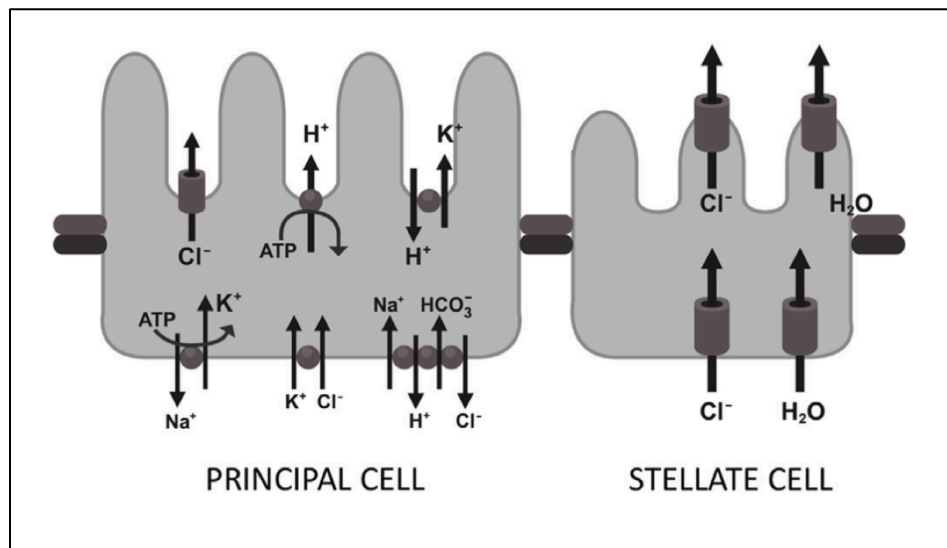
Figure 5: Schematic diagram depicting *Drosophila* principal and stellate cells, with their respective ion and solute co-transporters. Adapted with permission from Miller J. *et. al* 2013.

Additional parameters, that may be useful in elucidating the basic mechanisms governing

stone formation, such as ion electrophysiology, urine composition and pH can easily be

measured in the malpighian tubules using simple techniques such as the Ramsay

assay[118,120].

1.5.3   Current *Drosophila* Nephrolithiasis Research

Since the emergence of *Drosophila* as a novel model for human kidney stone disease, a

substantial body of literature has accumulated, utilizing the model in unique ways. Chen

et. al first described calcium oxalate nephrolithiasis by feeding the flies diets containing

the lithogenic agent's ethylene glycol, hydroxy-L-proline and sodium oxalate[121]. They

showed dose dependent calcium oxalate crystal deposition in the malpighian tubules after

feeding with the lithogenic diets. Potassium citrate, which complexes excess calcium,

reduced crystal deposition in the malpighian tubules. Similarly, Hirata *et. al* describe a

genetic model for calcium oxalate nephrolithiasis through selective knockdown of the

oxalate co-transporter SLC26A5 (*dPrestin*)[110]. Selective knockdown of the *dPrestin* gene

using the GAL4/UAS system reduced calcium oxalate stone formation in flies fed a

sodium oxalate diet, outlining the importance of oxalate metabolism and transport in

calcium oxalate stone formation. Melamine, a lithogenic agent notorious for having

caused kidney stone epidemics in dogs fed food accidentally laced with it, has also been

used to form calcium oxalate stones in *Drosophila*[122]. Recent work by Chi *et. al*, has

successfully produced xanthine nephrolithiasis in *Drosophila* by selective knockdown of

the enzyme *Xanthine dehydrogenase* (XDH) and identified the role of zinc in the

formation of Randall plaques[123]. Lang *et. al* recently described a uric acid model of

nephrolithiasis by selective knockdown of the *Uricase* enzyme in the malpighian tubules[124]. In *Drosophila*, purine metabolism leads to the formation of urate which is then converted to allantoin via the *Uricase* enzyme. GAL4/ UAS mediated knockdown of *Uricase* resulted in the accumulation of uric acid concretions in the malpighian tubules. This was mitigated with the use of drugs such as allopurinol. Other groups have been investigating the effects of commercially available drinks such as citrate containing juices and soft drinks in the *Drosophila* model of calcium oxalate nephrolithiasis[125,126]. Traditional Chinese medicinal plants have also been tested using the *Drosophila* model[127]. Potential drugs have also been tested. Landry *et. al* demonstrate reduced calcium oxalate stone deposition in the malpighian tubules with the administration of sulfate and thiosulfate, highlighting the importance of these compounds as competitive inhibitors of calcium oxalate crystalization[128].

1.6 Objectives & Research Aims

Objective 1: To develop a robust and reliable *Drosophila melanogaster* model for calcium oxalate nephrolithiasis.

Research Aim: Previous studies with the administration of lithogenic agents have reported varying results in regards to calcium oxalate stone deposition. Our goal is to identify the optimal lithogenic agent and its concentration, so as to reliably produce calcium oxalate stones in *Drosophila* malpighian tubules. We will use the lithogenic agent's ethylene glycol and sodium oxalate at concentrations of 0.05%, 0.1%, 0.5% and 1% *w/v* ratio, and measure stone burden using a combination of polarized light and fluorescent microscopy.

Objective 2: To develop *ex vivo* imaging capabilities using novel bisphosphonate based fluorescent probes.

Research Aim: Adequate visualization and quantification of stone burden remains a limiting factor in both animal and *Drosophila* models of human nephrolithiasis. Our laboratory has developed novel bisphosphonate based fluorescent probes that have previously been shown to bind calcium oxalate[129]. Use of these probes will allow us to visualize and quantify stone burden, plus serve as a starting point for optimizing *in vivo* imaging protocols.

Objective 3: Perform survival studies to characterize the effect of lithogenic diets on *Drosophila* life span.

Research Aim: Lithogenic agents cause calcium oxalate stone deposition by inducing a state of hyperoxaluria. At higher concentrations, these agents can be toxic. For our model to be useful we aim to characterize the effects of lithogenic agents on the life span of *Drosophila*. We will achieve this by performing survival studies on *Drosophila* fed varying concentrations of lithogenic diet. This will allow us to select the optimal concentration of lithogenic agent for our subsequent experiments.

Objective 4: To characterize *Drosophila* stone composition and morphology.

Research Aims: In order to accurately model human calcium oxalate nephrolithiasis, *Drosophila* stones must be similar in composition and morphology to human stones. We aim to isolate stone material from the malpighian tubules and characterize stone

composition/morphology using a combination of scanning electron microscopy and energy dispersive x-ray spectroscopy.

Objective 5: To develop novel intravital imaging techniques for studying stone formation *in vivo*.

Research Aims: A fundamental drawback in animal models of nephrolithiasis is the inability to visualize or quantify stone burden *in vivo*. Although the use of *Drosophila* simplifies this due to the ease of malpighian tubule dissection, developing intravital imaging techniques would be useful in tracking stone formation and quantifying the effect of potential interventions. We will develop a transgenic fly line that express red fluorescent protein in their malpighian tubules. Utilizing multi-channel resonance laser confocal microscopy, we will optimize and develop imaging protocols for visualizing the malpighian tubules *in vivo*. This will provide a sound platform for subsequent imaging protocols.

Objective 6: To develop a high-throughput noninvasive drug screening platform in the *Drosophila* model of human nephrolithiasis.

Research Aim: Current animal models do not allow for large scale high-throughput screening of potential therapies. We will screen an experimental drug library of 360 compounds that have been previously used as a basis for rational drug design[130]. Using our *Drosophila* model we will develop and validate a high-throughput noninvasive screening method by quantifying stone burden indirectly in the fly fecal matter. In the process we hope to identify compounds that antagonize calcium oxalate stone formation.

Chapter 2

2 Materials and Methods

This study did not require prior approval by the University of Western Ontario's animal use subcommittee, as the experimental use of *Drosophila melanogaster* is exempt from current ethics guidelines.

All *Drosophila melanogaster* stocks were obtained from the Bloomington Stock Center, Indiana, United States (http://flystocks.bio.indiana.edu), the Kyoto Stock Center, Kyoto, Japan (https://kyotofly.kit.jp/cgi-bin/stocks/index.cgi) and the National Institute of Genetics, Mishima, Japan (http://www.shigen.nig.ac.jp/fly/nigfly/).

2.1 *Drosophila melanogaster* Rearing

All *Drosophila melanogaster* stocks were reared in a dedicated *Drosophila* incubator (DT2-MP-47L Tritech Research Inc., Los Angeles, United States) at 22°C, 40% ambient humidity and a 12-12 hour light-dark cycle. *Drosophila melanogaster* stocks utilized in GAL4/UAS system experiments were reared at 29°C, 40% ambient humidity and a 12-12 hour light-dark cycle. All stocks were regularly inspected for signs of bacterial, fungal and mite infestations. Stocks were rotated to fresh food media every 4-5 days to prevent contamination, reduce competition between adult flies and larvae for food media, and to ensure an adequate supply of adult flies for experiments.

2.2   Preparation of Food Media

Drosophila food media was prepared manually in 1 liter batches on a bi-weekly schedule to avoid contamination and to ensure optimal freshness. After the media ingredients were weighed using a digital scale (Sartorius AG, Göettingen, Germany), they were mixed in distilled water and heated using a standard laboratory hot plate (Salton Appliances Corp., Dollard Des Ormeaux, Canada). The prepared media was then manually dispensed into wide polypropylene vials (32-114 Diamed Inc., Mississauga, Canada). The vials were allowed to rest for 8-12 hours to allow for adequate media solidification. It was noted that allowing the vials to rest for this period reduced moisture 'bleed' upon subsequent use of the food media. After resting, the vials were closed using dense cellulose acetate plugs (49-101 Diamed Inc., Mississauga, Canada) and labelled accordingly. All prepared food media was stored in a 4°C humidity controlled cold room until further use. Food media was stored for a period of 1 month after which unused media was discarded.

2.2.1   Standard Food Media

The standard Bloomington stock center recipe was used for the preparation of standard *Drosophila* food media. The ingredients required for the preparation of 1L of food medium are listed in **Table 1**.

	Ingredient	Amount
1	Distilled Water	1000 ml
2	*Drosophila* Agar (66-103 Diamed Inc.)	5.7 g
3	Inactive Yeast (62-106 Diamed Inc.)	19.3 g
4	Soy Flour (62-115 Diamed Inc.)	10 g
5	Yellow Corn Meal (62-100 Diamed Inc.)	73 g
6	Light Corn Syrup (62-117 Diamed Inc.)	75 ml
7	Acid Mix ¼ parts Propionic Acid (1368 Sigma Inc.) ¾ parts Phosphoric Acid (290017 Sigma Inc.)	5 ml
8	Optional: Tegosept 30% Solution (20-258 Diamed Inc.)	5 ml
	Total	1000 ml

Table 1: List of ingredients required for the preparation of standard *Drosophila* food media.

700 ml of distilled water was brought to a boil and agar added until it was well dissolved. Adequate cooking of the agar allowed for better solidification and adherence of the food media to the vial walls. This step was followed by the addition of yeast, soy flour and corn meal, and the solution allowed to simmer at medium heat for 10 minutes. 75 ml of corn syrup was mixed with the remaining 300 ml of distilled water and added to the solution and allowed to simmer for 5 minutes. 5 ml of acid mix was then added and the final solution left to cool to 60°C, after which it was ready to be dispensed into *Drosophila* vials. The acid mix of propionic acid and phosphoric acid work to inhibit

bacterial and fungal growth. Occasionally, the acid mix was substituted with 5ml of 30% Tegosept® solution for weaker strains prone to fungal overgrowth.

2.2.2　Lithogenic Food Media

The lithogenic agent's sodium oxalate (71800 Sigma Inc.) and ethylene glycol (324558 Sigma Inc.) were used to induce calcium oxalate stone formation in wild type Canton-S flies (Bloomington Stock # 1). Lithogenic diets containing these agents were prepared at concentrations of 0.05%, 0.1%, 0.5% and 1% *w/v*. The agents were thoroughly dissolved in water before the preparation of the food media using the recipe above.

2.3　*Drosophila* Lifespan Studies

In order to identify the optimal concentration of lithogenic agents for use in our subsequent experiments, lifespan studies were carried out to determine the relationship between lithogenic agent concentration, *Drosophila* lifespan and calcium oxalate stone burden. The standard protocol for *Drosophila melanogaster* life span measurement was used for this experiment[131].

2.3.1　Age Matching

To ensure all adult flies used for lifespan studies were of the same age and health, wild type Canton-S (Bloomington stock #1) were age matched. 100-150 adult wild type Canton-S were isolated in large egg collection cages (59-101 Diamed Inc.) over grape-juice agar plates **(Figure 6)**. A 1 cm wide dollop of active yeast paste (62-103 Diamed Inc.) was placed in the center of the grape-juice agar plates. Grape-juice agar stimulated

mating and provided a solid surface for the deposition of eggs. The dark red color of the agar contrasted well with the white eggs, allowing for better visualization and collection. The active yeast provided nutrition to the adult flies inside the egg collection cages. Eggs were allowed to collect on the surface of the agar plates for a day, after which they were replaced with a fresh plate and the old one discarded. This ensured that all subsequent eggs laid would be of approximately the same age. On the second day, the egg collection cages were opened and the adult flies discarded in an alcohol filled fly morgue. A cell scrapper was used to remove the central yeast, taking care not to damage or remove the deposited eggs. The surface of the grape juice agar plate was washed with 5 ml of PBS (Wisent Inc., St. Bruno, Canada) and a soft cotton bud was used to dislodge the deposited eggs. This egg/PBS suspension was then funneled into a 15 ml collection tube. The eggs were allowed to settle via gravity for 5 minutes and the supernatant removed from the tube. The settled egg 'pellet' was then washed with PBS at least twice or until the supernatant was clear. 100 μl of PBS was added to the washed eggs. 32 μl aliquots of this egg/PBS suspension was added to fresh room temperature standard media. Newly eclosed, age matched adult flies were collected after 10 days for use in lifespan experiments.
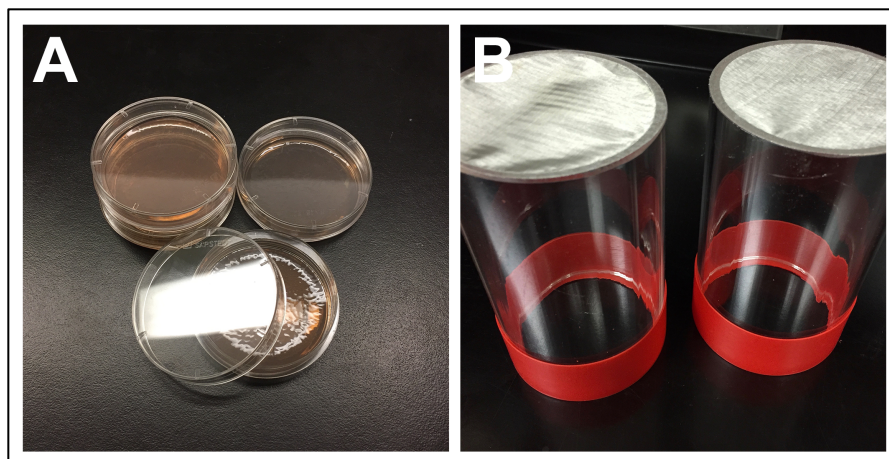
Figure 6: Grape-juice agar plates and egg collection cages used for age matching of *Drosophila melanogaster*.

2.3.1.1   Preparation of Grape-Juice Agar Plates

500 ml batches of grape-juice agar were prepared as required. The ingredients required for the preparation of grape-juice agar plates are listed in **Table 2**. Agar and sucrose was added to distilled water and heated until both were adequately dissolved. Grape-juice concentrate was then added and rigorously stirred. The solution was allowed to cool to 65°C, followed by the addition of ethanol and glacial acetic acid. Ethanol and glacial acetic acid inhibit bacterial and fungal growth. The solution was then poured into 100 mm plastic petri dishes (VWR Inc., Radnor, United States) and allowed to solidify at room temperature. The plates were subsequently labelled and stored in a 4°C cold room until further use.

	Ingredient	Amount
1	Distilled Water	375 ml
2	Bacteriological Agar (5306 Sigma Inc.)	12 g
3	Sucrose (7903 Sigma Inc.)	22 g
4	Grape Juice (Welch's grape-juice concentrate)	110 ml
5	Ethanol (Sigma Inc.)	10 ml
6	Glacial Acetic Acid (2183 Sigma Inc.)	5 ml
	Total	500 ml

Table 2: List of ingredients required for the preparation of grape-juice agar plates.

2.3.2 Lifespan Studies

30 age matched wild type Canton-S flies were anesthetized using CO_2 narcotization (Flystuff Inc., San Diego, United States) and added to lithogenic food media containing sodium oxalate (71800 Sigma Inc.). 4 test vials were used for each concentration (0.05 %, 0.1 %, 0.5% and 1 % w/v) of sodium oxalate. Wild type Canton-S flies in standard media were used as the baseline control. The flies were moved to new food media every 2-3 days to avoid competition between adult flies and larvae, which could potentially adversely affect survival. Deaths were recorded every day and any flies lost during transfer or adherent to the vial wall during transfer were censored. The recorded data was saved in a Microsoft excel file. The adult flies were followed till the last death or 40 days, whichever occurred first.

2.3.3   Statistical Analysis

The data generated by the life span studies was analyzed using the Statistical Package for Social Sciences (SPSS, Version 22.0.0.2 Mac, IBM Corp.). Life tables were constructed and a Kaplan-Meier survival analysis was performed. Statistical significance was tested using a log-rank test.

2.4   Development of Novel Imaging Modalities in *Drosophila*

This study aims to develop novel imaging modalities for visualizing and quantifying calcium oxalate stones in the *Drosophila melanogaster* model of human calcium oxalate nephrolithiasis. We have developed novel bisphosphonate based fluorescent probes that will bind to calcium oxalate calculi and allow us to image these calculi both *ex vivo* and *in vivo*. We have used a combination of polarized light, fluorescent microscopy and confocal microscopy to study stone formation.

2.4.1   Synthesis of Bisphosphonate Based Fluorescent Probes

All bisphosphonate fluorescent probes were designed and synthesized in collaboration with the Luyt Laboratory at the Department of Chemistry, Western University, London, Canada.

Bisphosphonates are well studied group of drugs known to tightly bind to hydroxyapatite and other calcium containing crystals. Several groups have conjugated the moiety to a fluorophore and it has previously been used to image the localization of bisphosphonate groups in bone and in microscopic stone fragments shed in the urine of patients with

calcium oxalate kidney stones[129,132]. Our imaging agent consists of the commercially

available bisphosphonate drug Alendronate conjugated to the fluorescent dye fluorescein

isothiocyanate (FITC) **(Figure 7)**. As a negative control, Notdronate was developed by

removal of the bisphosphonate group of Alendronate, leaving 4-amino-1-butanol

conjugated to the dye. All reagents were provided in powder form and stored in an

opaque container at −20°C to avoid photo-bleaching.
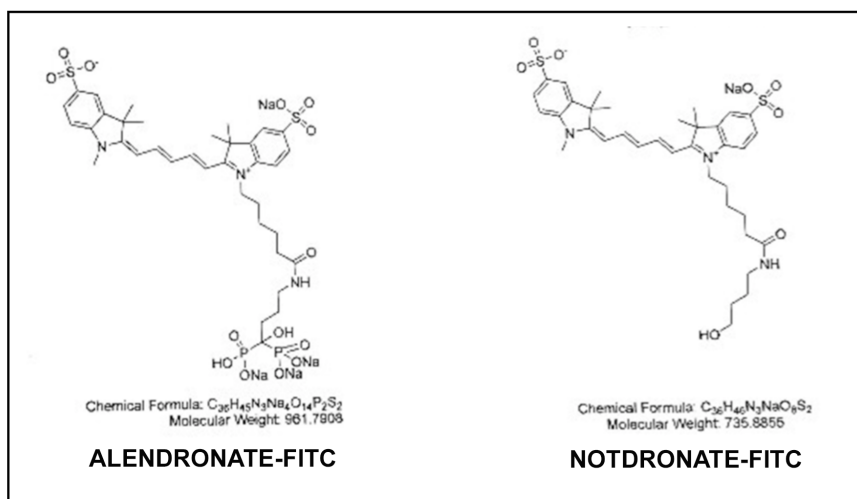
Figure 7: Molecular and chemical structure of novel bisphosphonate based fluorescent probes.

2.4.1.1   Synthesis of Alendronate-FITC

Sodium alendronate (34.0 mg, 106 μmol) was dissolved in saturated NaHCO3 (aq) (1

ml). Fluorescein (5/6) NHS ester (10 mg, 21 μmol) dissolved in DMF (100 μl) was added

and the solution stirred for 2 days in the dark. The product was dried, suspended in H2O

(1 ml) and dialyzed (cellulose ester, MWCO 0.1-0.5 kD) with water (3 X 500 mL). The

final product's concentration was determined by the UV absorption (ε493nm = 70,000

M- 1cm-1). The solution was subjected to RP-FCC (Isolera One, Biotage KP-C18-HS

12g cartridge) with a gradient from 0 to 30 % MeOH in H2O. The product was

lyophilized to yield FITC alendronate (8.6 μmol, 41 %) as an orange powder. UP LC-MS

(waters) method: 5-40% acetonitrile in water, both contain 0.1% formic acid, 3mins run;

Calculated m/z 608.07 (MH+), Found m/z: 608.10; RT (min) 1.40. Purity: >95%.

2.4.1.2   Synthesis of Notdronate-FITC

4-Amino-1-butanol (20 mg, 200 μmol) was dissolved in saturated NaHCO3 (aq) (1 ml).

Fluorescein (5/6) NHS ester (10 mg, 21 μmol) dissolved in DMF (100 μl) was added and

the solution stirred for 2 days in the dark. The reaction mixture was subjected to RP- FCC

(0 to 100 % MeOH in H2O) and the final product concentration was determined by the

UV absorption (ε493nm = 70,000 M-1cm-1). The solution was subjected to RP-FCC

(Isolera One, Biotage KP-C18-HS 12g cartridge) with a gradient from 0 to 25 % MeOH

in H2O. The product was lyophilized to yield fluorescein-4-butanol (4.8 μmol, 23 %) as

an orange powder. UP LC-MS (waters) method: 5-40% acetonitrile in water, both contain

0.1% formic acid, 3mins run; Calculated m/z 448.14 (MH+), Found m/z: 448.04; RT

(min) 2.23. Purity: >95%.

2.4.2   Specificity of Bisphosphonate Based Fluorescent Probes

To assess the specificity of our bisphosphonate based fluorescent probes to hydroxyapatite and calcium based stones, we subjected synthetic hydroxyapatite particles (289396 Sigma Inc.) and pulverized samples of infrared spectroscopy confirmed human calcium oxalate stones to bright field, polarized (TP-2, T-A2, Nikon Inc.) and fluorescent microscopy (TE-2000, Nikon Inc.) after staining with Alendronate-FITC, Notdronate-FITC and PBS as a control. The human stone sample was obtained from the hospital diagnostic laboratory and would otherwise have been discarded and destroyed. 50 mg of sample was incubated with 200 µl 0.1 mM Alendronate-FITC, 0.1 mM Notdronate FITC and PBS in an Eppendorf tube for 15 minutes. The sample was then centrifuged (Eppendorf Inc., Hamburg, Germany) at 15000 rpm for 5 minutes. The supernatant was removed and the underlying stone material was washed twice with distilled water in a similar fashion until the supernatant was clear. This ensured the removal of any unbound dye. 20 µl of sample suspended in distilled water was mounted on to glass slides with coverslips and imaged using brightfield, polarized light (TP-2, T-A2, Nikon Inc.) and fluorescent microscopy (TE-2000, Nikon Inc.).

2.4.3   Diet Induced Calcium Oxalate Stone Formation in
Drosophila

15-20 wild type Canton-S flies were added to wide vials containing either sodium oxalate media or ethylene glycol media at concentrations of 0.05%, 0.1%, 0.5%, 1% *w/v* of lithogenic agent. The flies were fed for a period of 14 days after which they were removed and processed for staining and imaging.

2.4.4   *Drosophila* Dissection Technique

Adult flies were euthanized by CO_2 narcotization (Flystuff Inc., San Diego, United

States) prior to dissection. All dissections were carried out under a dissecting microscope

(AmScope Inc., Irvine, United States) in a Sylgard (Dow Corning Inc., Michigan, United

States) lined Pyrex Petri dish (3160100 Sigma Aldrich Inc.). Sylgard lining provided

protection to the delicate *Drosophila* tissues and also the fine tips of the dissecting

forceps (Fine Science Tools Inc., Vancouver, Canada). Schneider's Media (0146 Sigma

Aldrich Inc.) was used as a dissection medium because its composition most closely

resembles the insect hemolymph and prevented osmotic cell lysis. A minimal touch

technique was used for dissection. The fly was anchored with fine forceps in the non-

dominant hand at the superior aspect of the thorax and submerged in the dissecting

media. Using forceps in the dominant hand, the anal region or terminalia, was grasped

below the final abdominal tergites and pulled gently. With gentle pressure the hindgut

emerged first followed by the anterior and posterior tubules. Occasionally, the hindgut

needed to be grasped to facilitate the descent of the malpighian tubules. After emergence

of the malpighian tubules the midgut was severed and the fly discarded. The tubules were

then processed for imaging.

2.4.5   *Ex vivo* Imaging of *Drosophila* Malpighian Tubules

Wild type Canton-S flies fed lithogenic diets for 14 days were removed, euthanized with

CO_2 narcotization and the malpighian tubules dissected. The tubules were then incubated

in 100 μl of 0.1 mM alendronate-FITC, 100 μl of 0.1 mM notdronate-FITC and PBS

respectively, for 15 minutes. Consequently, the dyes were removed and the tubules

washed several times with PBS to remove any unbound dye. Fine glass needles were used to transfer the tubules to poly-l-lysine coated microscope slides (P0425-72EA Sigma Inc.) for imaging. Brightfield, polarized light and fluorescent microscopy analysis was performed using an inverted microscope (TE-2000, Nikon Inc.). The steps of this experiment are demonstrated in schematic form in **Figure 8**.
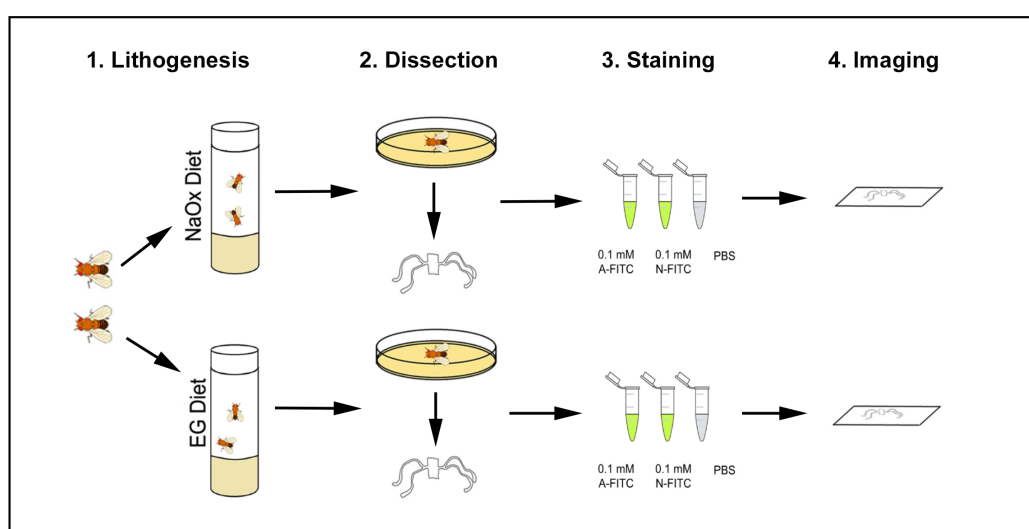
Figure 8: Schematic diagram demonstrating the stages in experimental design for *ex vivo* staining and imaging of *Drosophila melanogaster* malpighian tubules.

2.4.5.1   *Ex vivo* Imaging Analysis

All images were obtained with an inverted light microscope (Nikon Inc., Tokyo, Japan) using a 10x objective and analyzed using Image J software (NIH http://imagej.nih.gov). The image background was removed using the process > math > 'subtract' feature with a

value of 25. The images were sharpened with the process > math > 'unsharp mask'
feature, using a radius of 1 pixel and a mask weight of 0.60. Color threshold was adjusted
to white or green to outline birefringent or fluorescent crystals respectively. The analyze
> 'analyze particle' function was used to quantify the crystals using a pixel size of 0-
infinity, circularity of 0.00-1.00 and the outlines option checked. This analysis provided
us with the total particle count, average particle size and the area occupied by the
crystals. The data was statistically analyzed using Statistical Package for Social Sciences
(SPSS, Version 22.0.0.2 Mac, IBM Corp.).

2.4.6   *In vivo* Imaging of *Drosophila* Malpighian Tubules

Following the successful imaging of calcium oxalate stones in *ex vivo Drosophila*
malpighian tubes, we developed an innovative protocol for *in vivo* imaging. A transgenic
fly line expressing red fluorescent protein (RFP) was developed in order to visualize
malpighian tubules *in vivo*. Imaging this transgenic fly line allowed us to optimize our
imaging protocols for *in vivo* laser resonance confocal microscopy (Nikon Inc., Tokyo,
Japan).

2.4.6.1   Generation of RFP Expressing *Drosophila* Malpighian
Tubules

To create a transgenic fly line that expressed red fluorescent protein (RFP) in the
malpighian tubules, we used the established GAL4/UAS system for the genetic
manipulation of *Drosophila melanogaster*[115]. The GAL4/UAS system is a mating based
bi-partite system with spatio-temporal control. Two fly lines were obtained, one

expressing the yeast transcription activation factor (GAL4) in its malpighian tubules and

a second, which had an upstream activation sequence (UAS), followed by sequence

coding for the RFP protein. The progeny of this cross expressed both GAL4 which bound

the UAS sequence and drove gene expression, as illustrated in **Figure 9**. The driver

URO-GAL4 (Bloomington #44416) which expresses GAL4 in a urate oxidase pattern in

the principal cells of the malpighian tubules, was crossed with the responder line UAS-

RFP (Bloomington #32218) to produce a transgenic RFP expressing fly. This transgenic

line was reared at 29°C for optimal activation of the UAS/GAL4 system.
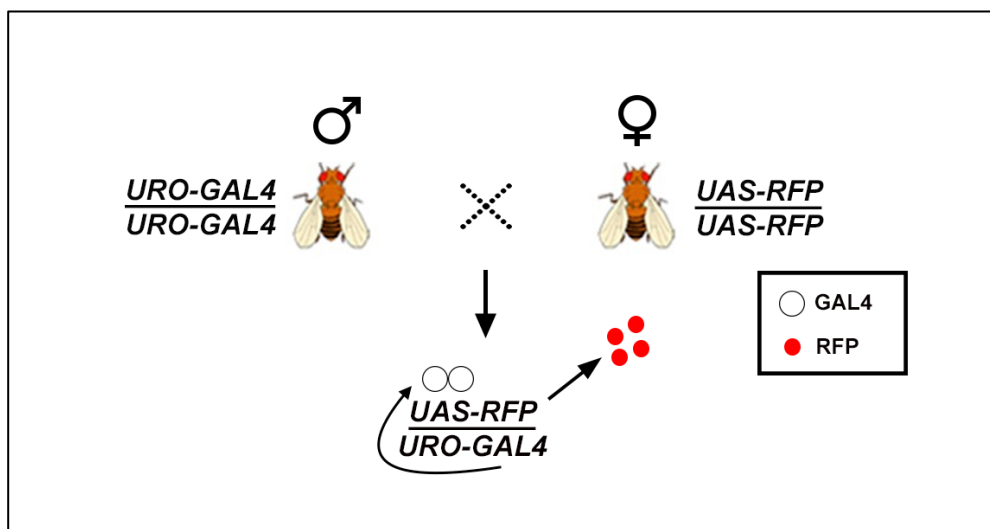
Figure 9: Schematic diagram depicting the GAL4/UAS cross resulting in progeny that expresses RFP in their malpighian tubules.

2.4.6.2   Intravital Confocal Microscopy

Transgenic RFP expressing flies were anesthetized using CO_2 narcotization. Imaging was carried out using 4x and 10x objective lenses. The DAPI (408 nm) channel was utilized to provide background contrast and the Alexa594 (594 nm) channel was used to outline the red fluorescent malpighian tubules. Pinhole was set to 1.2 AU and laser energy set to 115 with a gain of 18. Multichannel and z-stack images were taken using the NIS-Elements Advanced software (Nikon Inc., Tokyo, Japan) and analyzed with NIS-Elements Analysis software (Nikon Inc., Tokyo, Japan).

2.5   Elemental Analysis of Isolated *Drosophila* Stones

To adequately compare the composition of human stones to *Drosophila melanogaster* formed calcium oxalate stones, stone material formed by wild type Canton-S flies was isolated and analyzed using scanning electron microscopy and energy-dispersive x-ray spectroscopy to ascertain the elemental composition.

2.5.1   *Drosophila* Stone Isolation

150 wild type Canton-S flies were fed a 1% *w/v* sodium oxalate diet for 14 days. The flies were then transferred to an empty vial and euthanized with CO_2 narcotization (Flystuff Inc., San Diego, United States) for 10 minutes. These flies were dissected under a dissecting microscope (AmScope Inc., Irvine, United States) in Schneider's Media (0146 Sigma Aldrich Inc.) and the malpighian tubules removed. The dissected tubules were transferred to a 1 ml Eppendorf tube containing 1 ml of distilled water. The sample was centrifuged (Eppendorf Inc., Hamburg, Germany) at 15000 rpm for 5 minutes forming a

pellet of stone material and malpighian tubule tissue. The supernatant was carefully

pipetted out without disturbing the pellet. 0.5 ml of *Proteinase K* (5568 Sigma Inc.) at a

concentration of > 500 units/ml and 200 µl of 0.1% Triton-X (BDH Chemicals Inc.) was

added. *Proteinase K* performs optimally in the presence of a detergent. The pellet was

then broken up using a pipette and placed in a water bath at 37°C for 12-24 hours. After

this time, the Eppendorf tube was removed from the bath, inspected for dissolution of the

tissue and then centrifuged (Eppendorf Inc., Hamburg, Germany) at 15000 rpm for 5

minutes. The supernatant removed and the wash repeated 2-3 times to remove any

remaining organic material and impurities. The sample was then suspended in 500 µl of

distilled water for use in scanning electron microscopy and energy dispersive x-ray

spectroscopy analysis. At this point the sample could also be stored in a −80°C freezer for

analysis at a later date.

2.5.2   Scanning Electron Microscopy and Energy Dispersive X-ray Spectroscopy (SEM/EDX)

Scanning electron microscopy and energy dispersive x-ray spectroscopy analysis was

performed at Surface Sciences Western University, London, Ontario. 20 µl of isolated

stone sample suspended in distilled water was added to the surface of a 5 mm x 5 mm

silica wafer (Ted Pella Inc., Redding, United States) and air dried at 60°C for 2 hours.

The wafer and sample were then sputtered with a thin layer of gold to increase

conductivity for imaging. Scanning electron microscopy images were obtained with a

Hitachi S4500 Field emission SEM (Hitachi Inc., Tokyo, Japan) using a 15.0 kV electron

beam voltage. Energy dispersive x-ray spectroscopy analysis of the elemental

composition was done using a Quartz X One EDX System (Quartz Imaging Corporation, Vancouver, Canada). EDX graphs for elemental composition and atomic weight distribution of elements were obtained.

2.6 High-Throughput Drug Screening Platform

An experimental drug library containing 360 compounds was obtained through collaboration with Dr. Paul Spagnuolo at the School of Pharmacy, University of Waterloo, Waterloo, Canada. The experimental drug library is based on plant extracts with known regulatory activity in the human diet and has successfully been used as a starting point for rational drug design in previous studies[130,133]. The drug compounds were dissolved in DMSO and distributed into eight 96 well plates, in cohorts of 24 drugs per plate and stored in a −80 °C freezer until further use. A master list of the drugs and their concentrations were maintained in a Microsoft excel file for further reference. Drug screening was performed with an indirect approach to quantifying stone burden following treatment.

2.6.1 Assessment of DMSO on *Drosophila* Survival

Since our drug library used DMSO as a solvent, before the addition of drug compounds to the *Drosophila* diet, the effect of DMSO on the *Drosophila* survival was investigated. Four concentrations of DMSO 0.1%, 0.3%, 0.5% and 1% *w/v*, were evaluated to assess effects of DMSO on *Drosophila* survival using a similar protocol to the one described above.

2.6.2 Development of High-throughput Drug Screening Platform

Drosophila melanogaster have two pairs of malpighian tubules that coalesce into a common ureter and drain urine plus other materials into the gut at the junction between the mid and the hindgut. We observed that insects that form stones also excrete stone material into the fecal matter, providing an indirect means for assessing stone burden. Apart from feeding, most flies rest, mate and excrete on vertical surfaces such as the inside of the polypropylene fly vial.

A 0.5% *w/v* sodium oxalate diet was prepared based on our prior survival and stone burden data for the various lithogenic agents. This agent and concentration were chosen for drug screening due to the optimal balance between fly survival and stone burden. 200 μl of drug-DMSO solution was added to 5 ml of sodium oxalate food media during the preparation of the media to a final concentration of 10 μM. The drug was thoroughly mixed to ensure adequate distribution. Cohorts of 48 drugs were prepared for screening on a weekly basis. A 22 mm x 22 mm glass coverslip (C9802 Sigma Inc.) was inserted vertically into the cellulose acetate plug, where it served as a surface for flies to rest and excrete fecal matter. 30 Wild type Canton-S flies were added to the drug vials and allowed to feed for 7 days. Wild Type Canton-S flies in 0.5% sodium oxalate media without drug and standard media were used as controls. After 7 days, the flies were discarded and the glass coverslips with deposited fecal matter were subjected to polarized light and confocal microscopy (Nikon Inc., Tokyo, Japan). All images were analyzed using Image J software (NIH http://imagej.nih.gov) with a potential drug 'hit' considered

if birefringent stone material in the fecal matter was reduced by > 50 % as compared to

controls **(Figure 10)**.
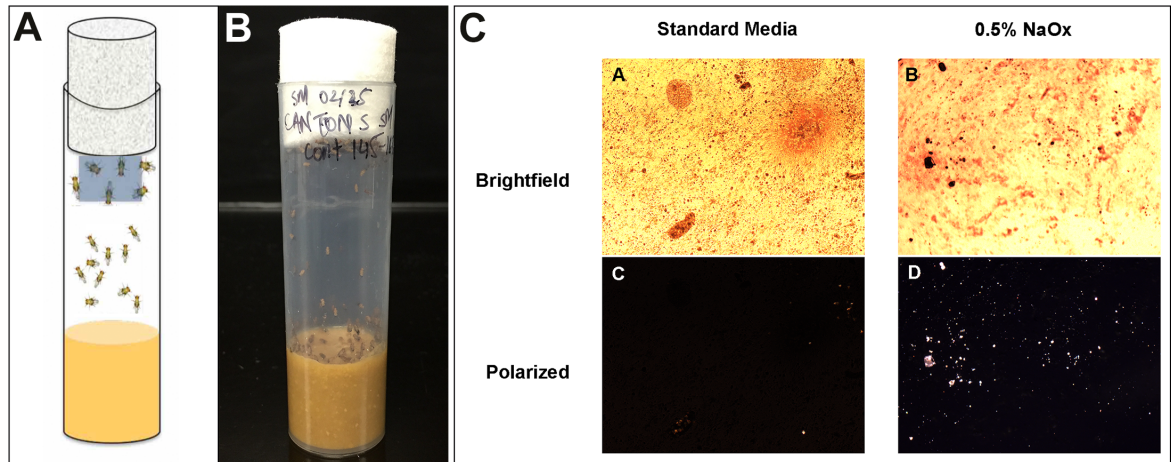
Figure 10: Diagram illustrating the drug screening vial setup, plus bright field and polarized microscopy of coverslips with *Drosophila* fecal matter laden with calcium oxalate stone material in the 0.5% *w/v* sodium oxalate group.

Chapter 3

3   Results

3.1 *Drosophila* Lifespan Studies

3.1.1   Survival in Sodium Oxalate Diet

Under standard laboratory conditions, the mean survival time for control wild type
Canton-S fed standard food media was 32.09 days **(Table 3)**. Sodium oxalate at a
concentration of 0.05% *w/v* did not adversely affect survival.

Means and Medians for Survival Time								
Diet Type	Mean[a]				Median[a]			
	Est.	Std. Err	95% CI		Est.	Std. Err	95% CI	
			Low.	Upp.			Low.	Upp.
Standard	32.09	.75	30.60	33.58	32.0	.96	30.10	33.89
NaOx 0.05%	31.59	1.13	29.37	33.80	33.0	1.63	29.80	36.19
NaOx 0.1%	27.32	.63	26.08	28.55	28.0	.33	27.33	28.66
NaOx 0.5%	21.58	.59	20.41	22.76	23.0	.44	22.12	23.87
NaOx 1%	15.11	.46	14.21	16.01	15.0	.44	14.12	15.87
Overall	23.70	.49	22.73	24.67	24.0	.58	22.85	22.14

**Table 3: Means and medians for survival of wild type Canton-S in varying concentrations
of sodium oxalate media. Estimation is limited to the largest survival time if it is censored.**

Increasing the concentration of sodium oxalate to 0.1% and 0.5% *w/v* resulted in a 14.8% and 32.7% reduction in survival respectively. A 1% *w/v* concentration of sodium oxalate caused a 52.9% reduction in survival as compared to controls, with a mean life span of 15.12 days. A Kaplan Meier survival analysis of wild type Canton-S fed varying concentrations of sodium oxalate is illustrated in **Figure 11**.
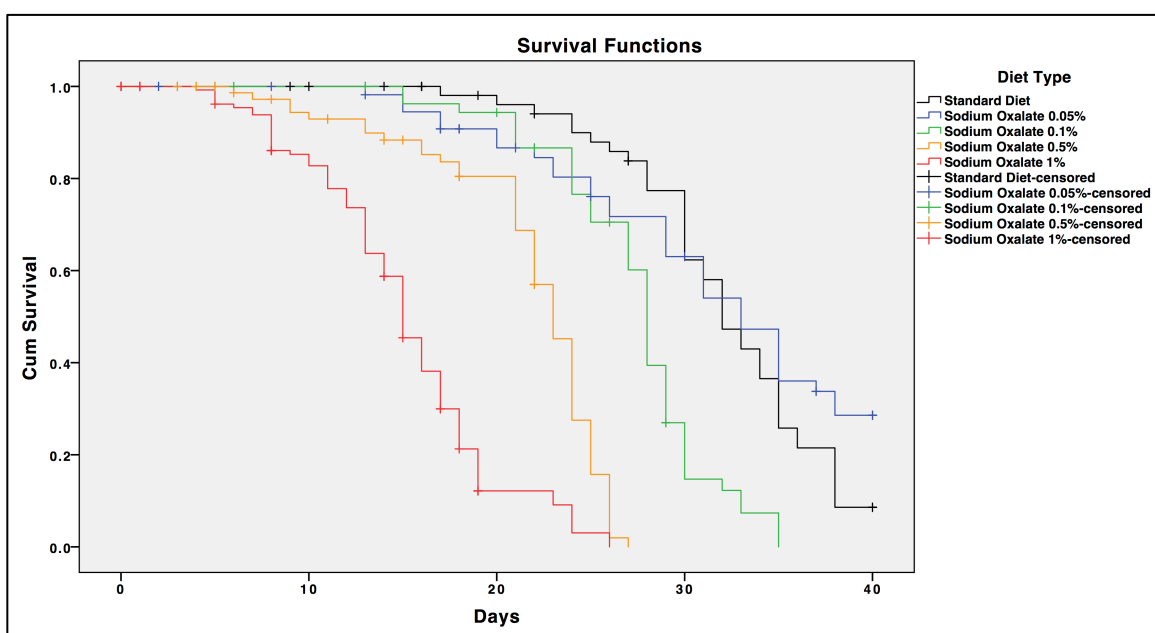
Figure 11: Kaplan Meier survival analysis of wild type Canton-S fed various concentrations of the lithogenic agent sodium oxalate for a period of 40 days.

Both male and females survived for an average of 32 days on standard food media. Interestingly, females on a 0.05% *w/v* sodium oxalate diet survived for longer (34.07 days) as compared to males fed a similar diet or standard diet. Male flies fed a 0.1% *w/v* sodium oxalate diet survived for an average of 1.64 days longer than females fed a

similar diet. No statistically significant differences in survival between sexes was observed for 0.5% and 1% *w/v* sodium oxalate diet. A Kaplan Meier analysis comparing survival between male and female wild type Canton-S is illustrated in **Figure 12**.
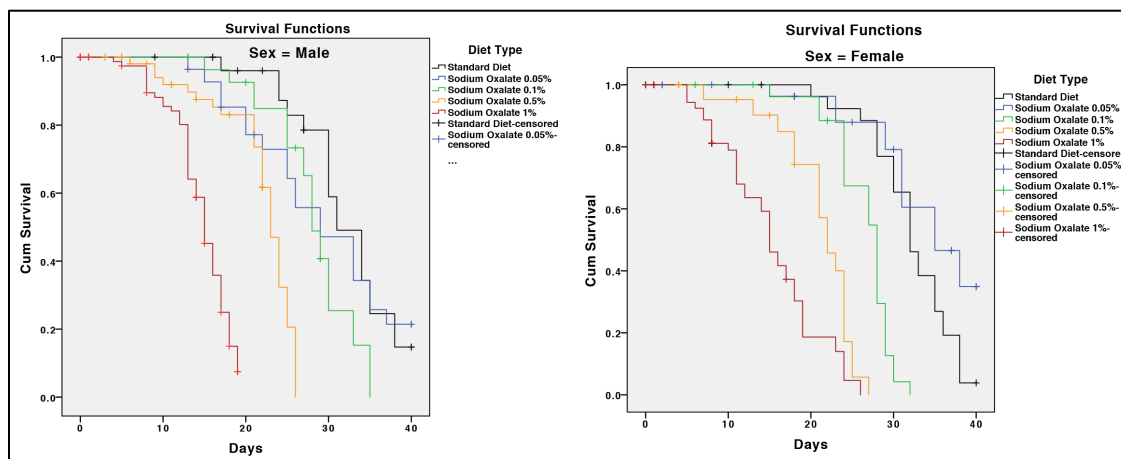
Figure 12: Kaplan Meier survival analysis of male and female wild type Canton-S fed various concentrations of the lithogenic agent sodium oxalate for a period of 40 days.

A log-rank test revealed a statistically significant (p value < .0001) difference in survival between wild type Canton S fed increasing concentrations of the lithogenic agent sodium oxalate **(Table 4)**.

	Chi-square	df	Sig.
Log-Rank (Mantel Cox)	327.547	4	< .0001
Breslow (Generalized Wilcoxon)	257.578	4	< .0001
Tarone-Ware	290.168	4	< .0001

Table 4: Statistical analysis of the survival distributions for the different *Drosophila* diet types.

3.2 Development of Novel Imaging Modalities in *Drosophila*

To develop imaging modalities in the *Drosophila melanogaster* model of human calcium oxalate nephrolithiasis, the novel bisphosphonate based fluorescent probes Alendronate-FITC and its negative control Notdronate-FITC were developed for *ex vivo* imaging.

3.2.1 Specificity of Bisphosphonate Based Fluorescent Probes

To assess the specificity of our bisphosphonate based fluorescent probes to hydroxyapatite and calcium containing stones, we subjected synthetic hydroxyapatite particles **(Figure 13)** and pulverized samples of infrared spectroscopy confirmed human calcium oxalate stones **(Figure 14)** to bright field, polarized light and fluorescent microscopy.
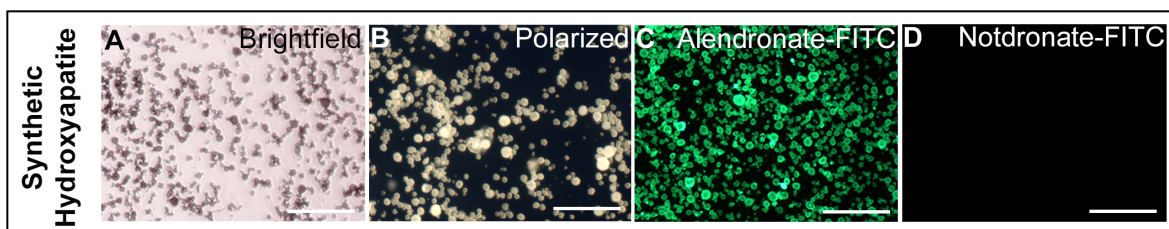
Figure 13: Synthetic hydroxyapatite subjected to brightfield, polarized light and fluorescent microscopy after straining with alendronate-FITC and notdronate-FITC. Scale bars = 100 μm

Both synthetic hydroxyapatite and pulverized human calcium oxalate stones showed brilliant birefringence under polarized light **(Figure 13 B, Figure 14 B)**. Synthetic hydroxyapatite particles stained with Alendronate-FITC exhibited high fluorescent signal intensity **(Figure 13 C)** when subject to a 488 nm wavelength blue FITC laser, as compared to those stained with Notdronate-FITC **(Figure 12 D)**.
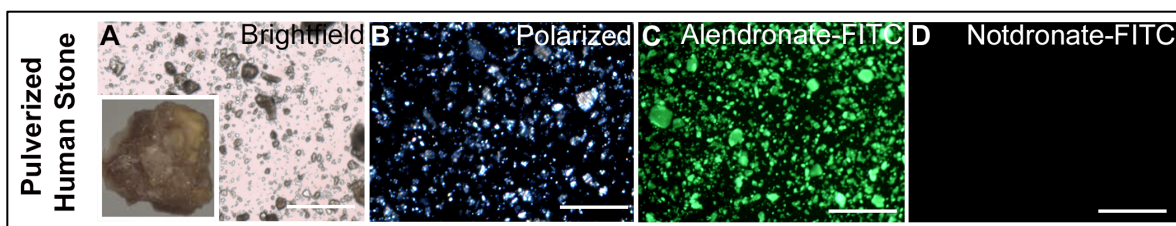
Figure 14: Pulverized calcium oxalate human stone sample subjected to brightfield, polarized light and fluorescent microscopy after straining with alendronate-FITC and notdronate-FITC. Scale bars = 100 μm

Similar results were obtained with the pulverized human calcium oxalate stone sample **(Figure 14 C, Figure 14 D)**, suggesting that Alendronate-FITC selectively binds to hydroxyapatite and calcium containing stones.

3.2.2   *Ex vivo* Imaging of *Drosophila* Malpighian Tubules

Wild type Canton-S were used for this experiment. 20-30 flies were added to lithogenic diets containing sodium oxalate or ethylene glycol at concentrations of 0.05%, 0.1%, 0.5% and 1% *w/v* for a period of 14 days. The malpighian tubules were subsequently dissected and stained with Alendronate-FITC or Notdronate-FITC. Images were taken with polarized light and fluorescent microscopy **(Figure 15, Figure 16)**.

3.2.2.1   Sodium Oxalate Diet

Wild type Canton-S fed a sodium oxalate diet, under polarized light exhibited brilliant birefringence throughout the anterior and posterior malpighian tubules with finer crystals scattered throughout **(Figure 15 A, B, C, D)**. At lower concentrations of 0.05% and 0.1% *w/v* sodium oxalate the calculi are deposited in the initial segments of the malpighian tubules **(Figure 15 A, B)**. At higher concentrations of 0.5% and 1% *w/v* sodium oxalate fine calculi can be seen occupying the whole malpighian tubule, specifically concentrated in the main segments of the tubule **(Figure 15 C, D)**.
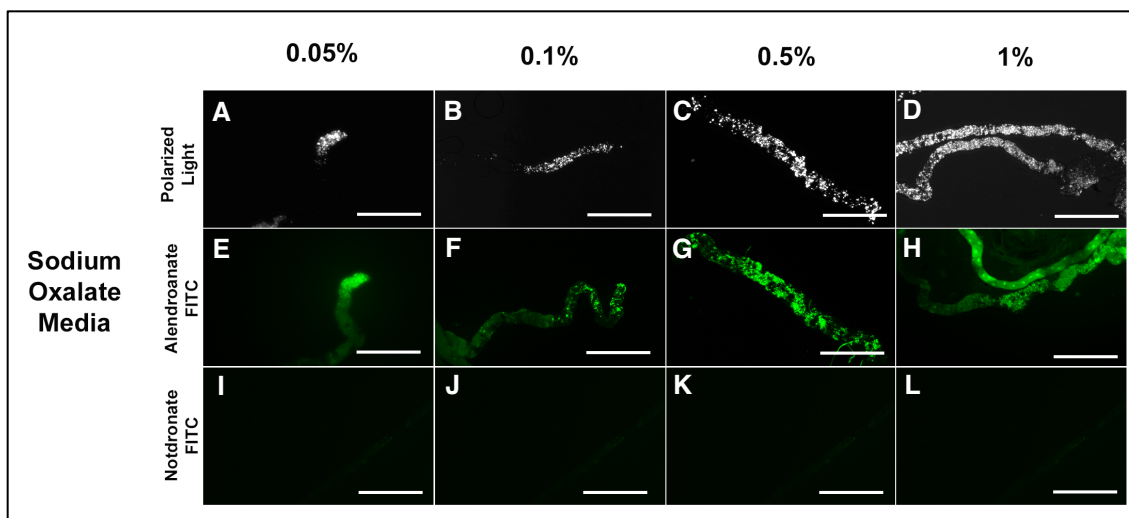
Figure 15: Polarized light and fluorescent microscopic analysis of malpighian tubules following feeding with various concentrations of sodium oxalate. Scale bars = 100 μm

Malpighian tubules from wild type Canton-S stained with Alendronate-FITC exhibit a fluorescent signal that closely corresponds to the areas of birefringence shown by polarized light microscopy **(Figure 15 E, F, G, H)**. Fluorescent signal intensity is concentrated in the initial parts of the malpighian tubule for 0.05% and 0.1% *w/v* sodium oxalate **(Figure 15 E, F)**. At higher concentrations of 0.5% and 1% *w/v* sodium oxalate fluorescent signal is observed throughout the tubule lumen **(Figure 15 G, H)**. Signal intensity increased with increase in sodium oxalate dosage. Tubules stained with Notdronate-FITC did not reveal any fluorescent signal **(Figure 15 I, J, K, L)**.

3.2.2.2   Ethylene Glycol Diet

Wild type Canton-S fed an ethylene glycol diet exhibited a more scattered pattern of birefringence in the malpighian tubules, as compared to the sodium oxalate diet. At lower concentrations of 0.05% and 0.1% *w/v* ethylene glycol calculi can be seen scantily

dispersed throughout the malpighian tubule and not restricted to the initial segments **(Figure 16 A, B)**. At higher concentrations of 0.5% and 1% *w/v* ethylene glycol the distribution of calculi is denser, with more calculi concentrated in the main segment of the tubule **(Figure 16 C, D)**.
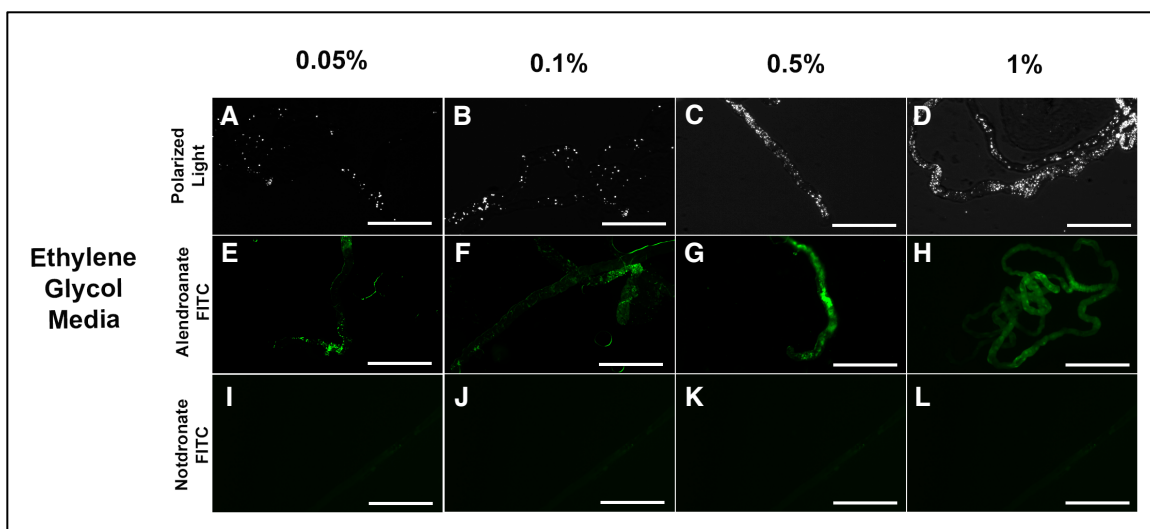
Figure 16: Polarized light and fluorescent microscopic analysis of malpighian tubules following feeding with various concentrations of ethylene glycol. Scale bars = 100 μm

Flies fed a 0.05% and 0.1% *w/v* ethylene glycol and stained with Alendronate-FITC, exhibited similar scanty fluorescent signal intensity throughout the malpighian tubule **(Figure 16 E, F)**. At higher concentrations of 0.5% and 1% *w/v* ethylene glycol there is a strong fluorescent signal throughout the tubule, especially the main segments **(Figure 16 G, H)**. Notdronate-FITC again does not exhibit fluorescent signal at any concentration of lithogenic diet **(Figure 16 I, J, K, L)**.

3.2.2.3   Statistical Analysis

Wild type Canton S fed a sodium oxalate diet formed calcium oxalate calculi that were on average 4.96 μm in size. Flies fed an ethylene glycol diet produced calculi that were approximately 59.5% (12.25 μm) larger than those fed the sodium oxalate diet, however, these calculi were distributed haphazardly throughout the tubule.
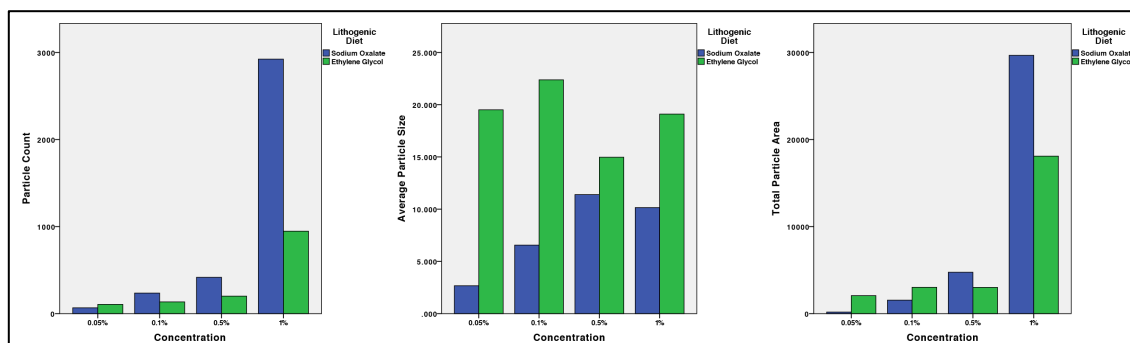
Figure 17: Polarized light microscopy group: Comparison between tubule stone count, average stone size & total area of tubule occupied in flies fed varying concentrations of sodium oxalate & ethylene glycol.

Flies fed either the sodium oxalate diet or ethylene glycol diet showed an increase in stone burden in response to increase in lithogenic agent concentration **(Figure 17)**. However, the sodium oxalate diet group showed a more linear response and stone distribution throughout the malpighian tubule. Increasing the concentration of sodium oxalate to 0.5% and 1% *w/v* resulted in a 6-fold and 43-fold increase in stone count as compared to 0.05% *w/v*. Ethylene glycol showed more modest results, with a 2-fold and 9-fold increase in stone count at concentrations of 0.5% and 1% *w/v* respectively.

Fluorescent signal intensity data for both groups is illustrated in **Figure 18**.
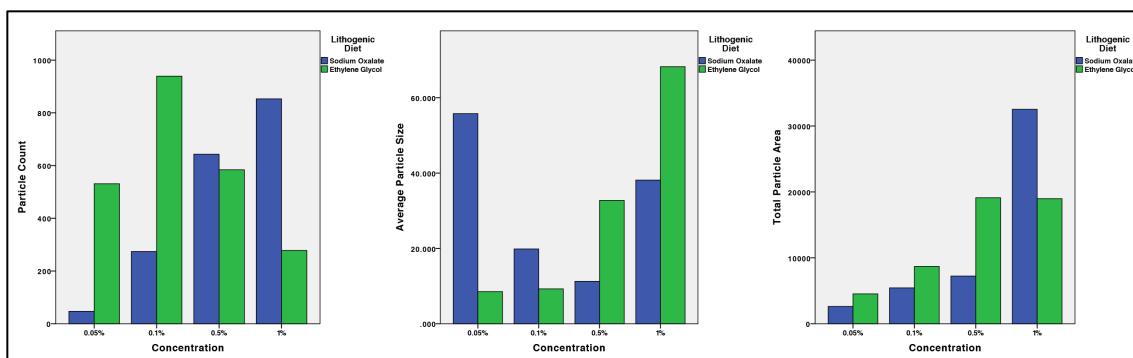
Figure 18: Fluorescent microscopy group: Comparison between tubule stone count, average stone size & total area of tubule occupied in flies fed varying concentrations of sodium oxalate & ethylene glycol.

3.2.3 *In vivo* Imaging of *Drosophila* Malpighian Tubules

Transgenic flies and larvae expressing RFP in the malpighian tubules were imaged using dual laser fluorescence confocal microscopy.

3.2.3.1 Intravital Confocal Microscopy

Immobilized transgenic RFP expressing larvae showed bright red malpighian tubules that were clearly visible through the larval fat body **(Figure 19 A)**. No malpighian tubules were visible in control wild type Canton-S larvae. Fine peristaltic movements of the tubules in the hemolymph were visible. The DAPI channel provided adequate contrast to the red fluorescent malpighian tubules allowing them to be visualized in their entirety **(Figure 19 A, Figure 19 B)**. Minimal amount of red auto-fluorescence was present in the Alexa 594 channel **(Figure 19 C)**.
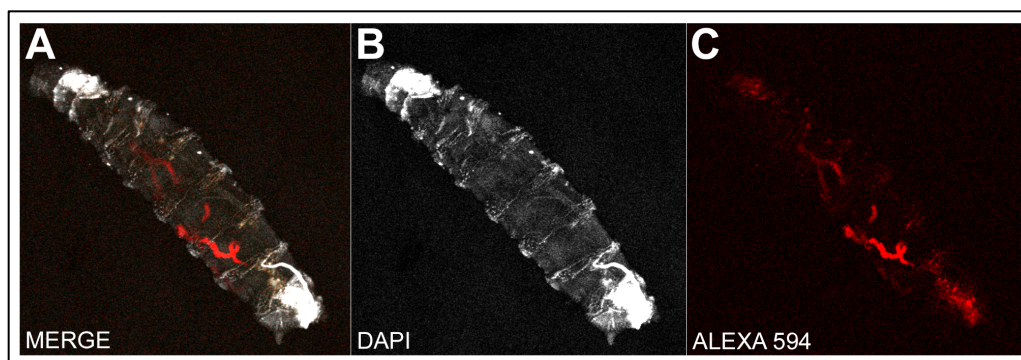
Figure 19: (A) Intravital imaging of live *Drosophila* larvae expressing RFP in the malpighian tubules using dual channel (B) DAPI & (C) Alexa 594 laser confocal microscopy.

Bright red anterior and posterior malpighian tubules were clearly visualized in the thoraco-abdomen of adult transgenic RFP expressing *Drosophila* group **(Figure 20)**. No malpighian tubules were visible in the wild type Canton-S control group. Imaging was easier with the insect in supine position as compared to other orientations. The DAPI channel provided good contrast to the exoskeleton and external fly structures, allowing for the visualization of RFP tubules **(Figure 20 A, Figure 20 B)**. Minimal auto-fluorescence, except for the eyes, was seem in the adult fly **(Figure 20 C)**.
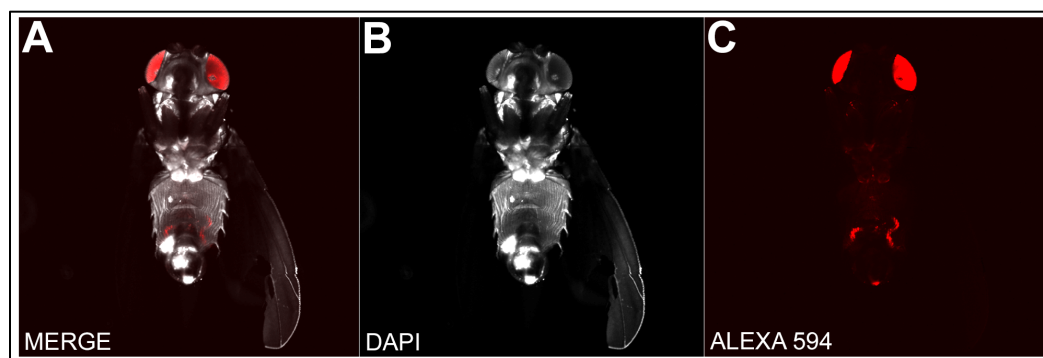
Figure 20: (A) Intravital imaging of live adult *Drosophila* expressing RFP in the malpighian tubules using dual channel (B) DAPI & (C) Alexa 594 laser resonance confocal microscopy.

3.3   Elemental Analysis of *Drosophila* Stones

3.3.1   Scanning Electron Microscopy & Energy Dispersive X-ray Spectroscopy

SEM images revealed calcium oxalate calculi with sizes ranging between 6 to 16 μm, often exhibiting spectacular shapes and configurations **(Figure 21 A, Figure 22 A)**. Two composition types, calcium oxalate monohydrate **(Figure 21, Figure 23)** and calcium oxalate dihydrate **(Figure 22)** were predominately present in the sample. Calcium oxalate monohydrate crystals, also known whewellite, exhibit the classic dumbbell shaped crystals **(Figure 21 A)** similar to crystals observed in human urine samples. While calcium oxalate dihydrate or weddellite, exhibited the classic envelope shaped crystals **(Figure 22 A)**.
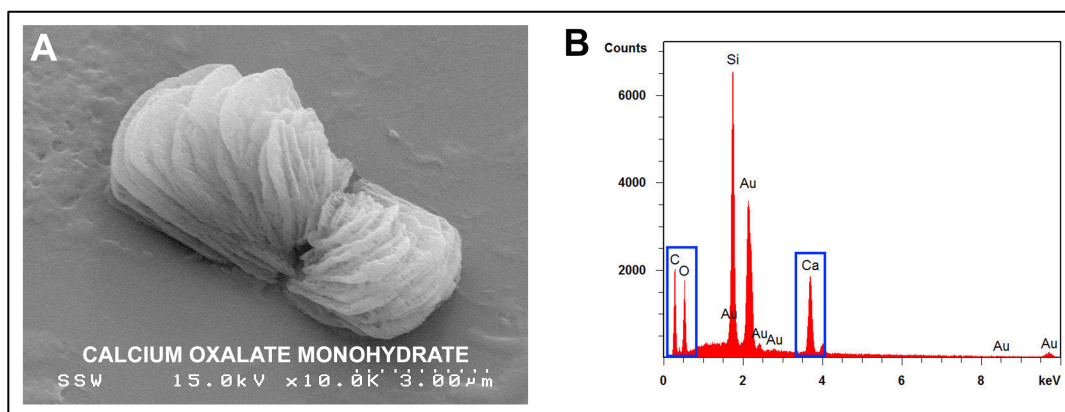
Figure 21: (A) Scanning electron micrograph of *Drosophila* calcium oxalate monohydrate stone. (B) Graphical representation of EDX analysis showing elemental distribution in *Drosophila* calcium oxalate monohydrate stone.

Energy dispersive x-ray spectroscopy analysis of the isolated stones revealed peaks of

calcium **(Figure 21 B, Figure 22 B, Figure 23 B)** plus peaks of carbon and oxygen in

ratios of 1:1 **(Figure 21 B)** and 1:2 **(Figure 22 B)**. The peaks of gold and silicon relate to

the underlying silica wafer on which the sample was mounted and surface sputtering of

gold during preparation of the sample.
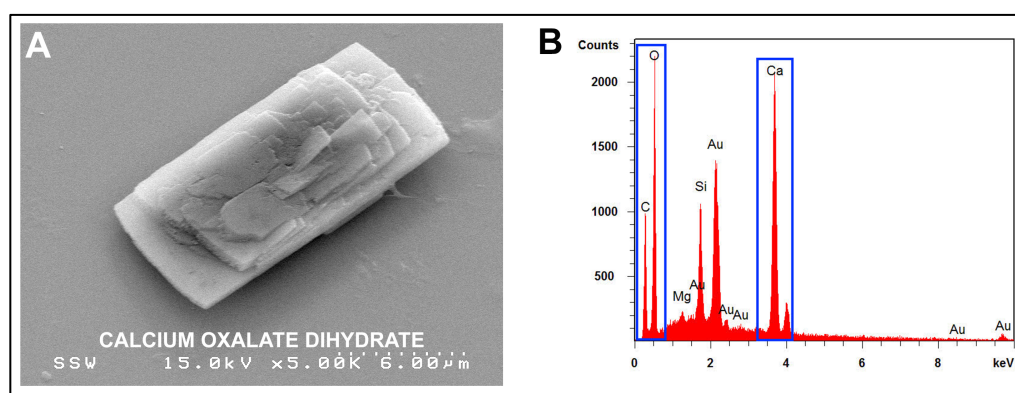
Figure 22: (A) Scanning electron micrograph of *Drosophila* calcium oxalate dihydrate stone. (B) Graphical representation of EDX analysis showing elemental distribution in *Drosophila* calcium oxalate dihydrate stone.

Occasionally, some calculi showed the presence of small amounts of magnesium **(Figure 22 B, Table 5)**, similar to human calcium oxalate stones[134].
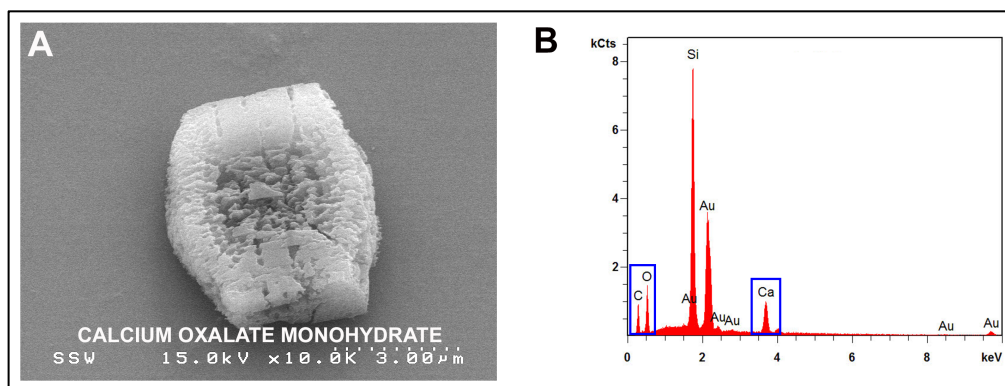
Figure 23: (A) Scanning electron micrograph of *Drosophila* calcium oxalate monohydrate stone. (B) Graphical representation of EDX analysis showing elemental distribution in *Drosophila* calcium oxalate monohydrate stone.

The atomic weight distributions of elements present in stones isolated from *Drosophila Melanogaster* tubules are listed in **Table 5**. Carbon and oxygen are the predominant elements and occur in a similar distribution as compared to human stone samples analyzed by energy dispersive x-ray spectroscopy[134].

Atomic Weight Percentages	Calcium	Carbon	Oxygen	Magnesium
Calcium Oxalate Monohydrate	8.72	43.11	48.17	0.00
Calcium Oxalate Dihydrate	10.71	27.64	61.35	0.30
Calcium Oxalate Monohydrate	8.18	34.81	57.01	0.00
Human Stone Sample[134]	18.17	31.71	24.33	1.67

Table 5: Energy dispersive x-ray spectroscopy analysis of *Drosophila* stones demonstrating the elemental distribution in atomic percentages.

A comparison between the relative size of calcium oxalate stones **(Figure 24 B, solid arrow)** to the malpighian tubule lumen **(Figure 24 B, dashed arrow)** is illustrated in the SEM image below. Large stones obstructing the common ureter were occasionally seen in flies fed lithogenic diets **(Figure 24 A)**.
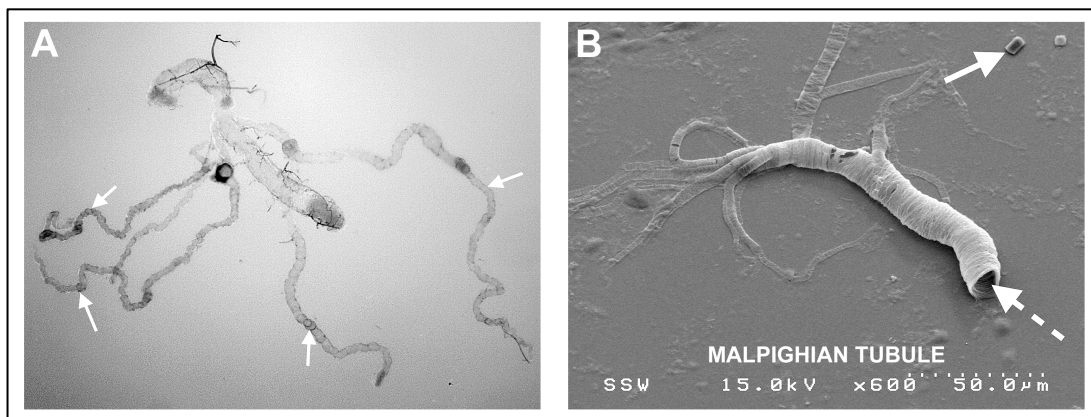
Figure 24: (A) Light microscope image demonstrating the four malpighian tubules (arrows) with a large central stone lodged in the ureter. (B) Scanning electron micrograph of a *Drosophila* malpighian tubule (dashed arrow) and *Drosophila* stones (solid arrow).

3.4   High-throughput Drug Screening Platform

Due to the anatomical relationship of *Drosophila* malpighian tubules to the gut, flies drain urine and other materials into the fecal matter. We have developed a non-invasive high-throughput screening method to measure stone burden in the fecal matter using polarized and confocal microscopy. We use this novel screening method to screen through a library of 360 experimental drugs to identify compounds that reduce calcium oxalate stone formation.

3.4.1   Assessment of DMSO on *Drosophila* Survival

The average life span of flies fed a 0.1% and 0.3% *w/v* DMSO diet was 38 and 36 days respectively. This was similar to the life span of 40 days in control wild type Canton-S fed a standard diet. Life span at concentrations of 0.5% and 1% *w/v* DMSO was reduced

to 25 days and 15 days respectively. At concentrations higher than 0.3% *w/v* of DMSO, time to eclosion was prolonged, with an overall reduction in fly life span. These results are in line with previous literature[135].

3.4.2 Development of High-throughput Drug Screening Platform

Dual channel confocal microscopy with polarized transmitted light was used for analysis of *Drosophila* fecal matter deposited onto glass coverslips. EGFP and Alexa594 were used for background fluorescence to provide contrast for calcium oxalate stone material. Two control groups, one fed a standard diet and another a 0.5% *w/v* sodium oxalate diet were analyzed at the start of the experiment to produce baseline controls. Wild type Canton-S flies fed a standard diet did not show the presence of any calcium oxalate stone material in the fecal matter as shown in **Figure 25**.
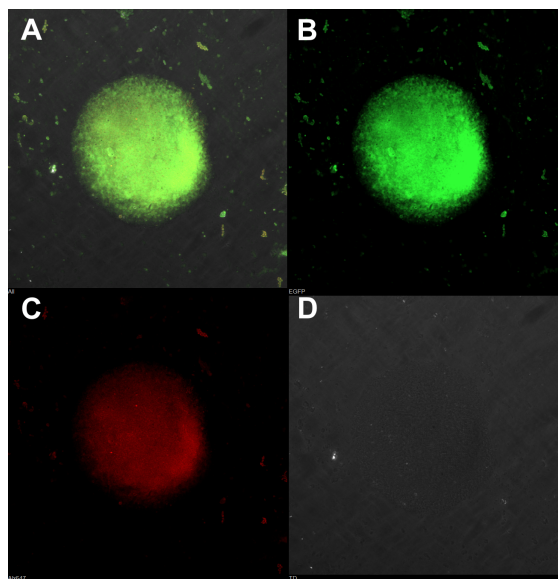
Figure 25: (A,B,C) Confocal and (D) polarized light analysis of fecal matter from flies fed a standard diet. (A) Merged image of GFP, Alexa594 and polarized light channels show no presence of calcium oxalate stone material.

Wild type Canton-S control group fed a 0.5% *w/v* sodium oxalate diet showed numerous calcium oxalate crystals in the fecal matter as shown in **Figure 26**. Stone size and morphology were similar to those isolated directly from the malpighian tubules in our scanning electron microscopy and energy dispersive x-ray spectroscopy analysis. This suggests that intact stone material is excreted into the fecal matter via the malpighian tubules. The EGFP and Alexa594 provided adequate background contrast to the fecal matter allowing for the visualization and quantification of stone material.
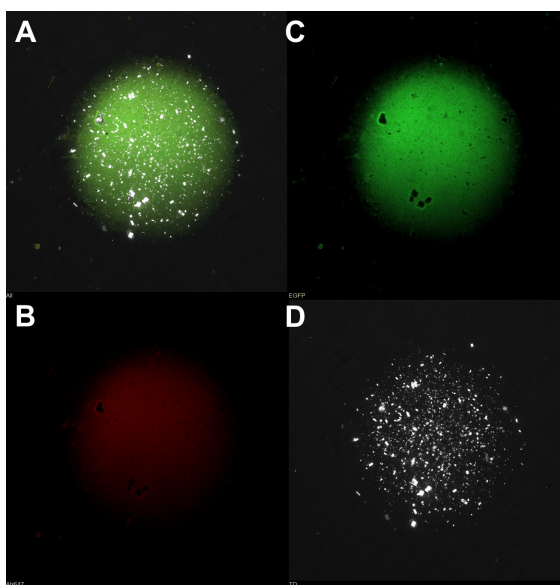
Figure 26: (A,B,C) Confocal and (D) polarized light analysis of fecal matter from flies fed a 0.5% *w/v* sodium oxalate diet. (A) Merged image of GFP, Alexa594 and polarized light channels show abundant calcium oxalate crystals in the fecal matter.
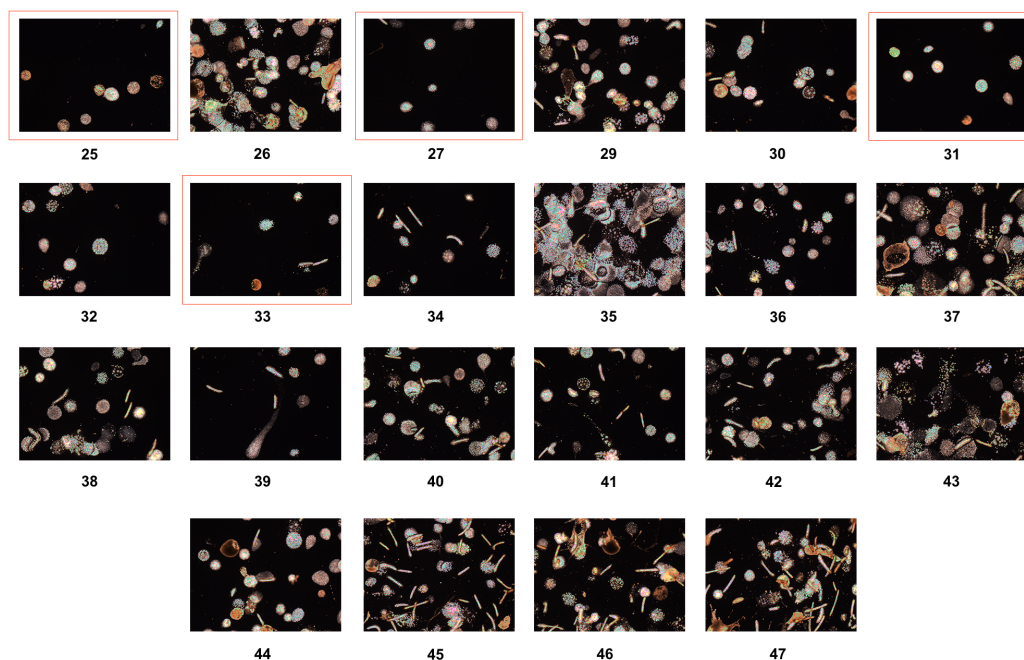
Figure 27: Polarized light microscopy images of fecal matter from stone forming
***Drosophila* fed a panel of 24 drugs. Potential 'hits' are outlined in red.**

Following the establishment of our control groups, cohorts of 24 drugs were tested per week and analyzed using polarized light microscopy **(Figure 27)**. A drug was considered a 'hit' if stone formation was reduced by > 50% compared to our control groups. Drugs that caused toxicity or reduction in life span were re-evaluated at a lower concentration. Drugs that were considered potential 'hits' were re-evaluated through direct visualization and quantification of stone burden in malpighian tubules following dissection.

A total of 6 drugs compounds that reduced calcium oxalate stone formation were identified and are outlined in **Table 6.**

	Drug 'Hits'
1	Aloin B
2	Alpha-mangostin
3	Apiin
4	Arbutin
5	Cucurbatacin B
6	Isorhamnetin

Table 6: List of drugs that reduce calcium oxalate stone formation in the *Drosophila* model of human nephrolithiasis.

Chapter 4

4　Discussion and Conclusions

In this project we demonstrate the versatility and advantages of *Drosophila melanogaster* as a novel model for human nephrolithiasis. We highlight the ease with which calcium oxalate stones are formed, in a highly reliable fashion, through simple dietary manipulation. Furthermore, we demonstrate new imaging modalities for measuring stone burden both *in vivo* and *ex vivo*. We have identified 6 compounds, from a large scale screen of 360 experimental drug compounds, that inhibit calcium oxalate stone formation.

4.1　*Drosophila* Life Span Studies

An ideal model for kidney stone disease should be simple, amenable to imaging and have an adequate life span to provide sufficient time to study stone formation or test the effect of a therapeutic agent. Lithogenic agents such as sodium oxalate and ethylene glycol act by producing a state of hyperoxaluria. Sodium oxalate is a potent source of oxalate and ethylene glycol serves as a precursor for oxalate formation. However, these lithogenic agents can also be toxic. For our model to be useful we decided to carry out life span studies in order to identify the optimal concentrations of lithogenic agents for use in subsequent experiments. Sodium oxalate was chosen as a lithogenic agent of choice due to our *ex vivo* imaging results which showed that sodium oxalate produced calcium oxalate stones in a more linear fashion compared to ethylene glycol.

A mean survival time of 32.09 days in the control wild type Canton-S group was in line with lifespans reported in other studies. Sodium oxalate at concentrations of 0.05% *w/v* did not adversely affect survival. Surprisingly, female flies fed sodium oxalate at this concentration survived for longer than the control group. A larger sample size is needed to validate this trend. At 0.05% *w/v* sodium oxalate, the flies produced minimal calcium oxalate stones and hence this concentration was not used for any of our subsequent experiments. At 0.1% *w/v* and 0.5% *w/v* sodium oxalate the flies survived for 27.32 and 21.58 respectively. At these concentrations wild type Canton-S flies produced stones throughout the main segment of the malpighian tubules. Both these concentrations are considered suitable for *ex vivo* and *in vivo* imaging as they produced an adequate stone burden. A 0.5% *w/v* concentration of sodium oxalate was used for our high throughput drug screening platform. The average life span of 21 days provided an adequate time frame for assessing the effects of the experimental drugs on stone burden. At 1% *w/v* sodium oxalate fly survival was severely affected with an average survival time of 15.11 days. This concentration of sodium oxalate was used in the SEM/EDX analysis experiment as the flies produced the maximum amount of stones allowing for better stone isolation and sample yield. This concentration is not recommended for drug screening or imaging purposes. There was no difference in survival or stone burden between sexes, hence sex segregation was not required for any of our subsequent experiments.

4.2 Development of Novel Imaging Modalities in *Drosophila*

One of the main drawbacks of current animal models of nephrolithiasis is difficulty in monitoring stone burden. We describe the superiority of the *Drosophila* model which is

amenable to both *ex vivo* and *in vivo* visualization and quantification of stone burden. We repurposed the bisphosphonate Alendronate and conjugated it to the fluorophore fluorescein isothiocyanate. We also developed a negative control Notdronate, that is similar to Alendronate but lacks the functional bisphosphonate ring. Bisphosphonates bind strongly to calcium and hydroxyapatite allowing for visualization and quantification of stone burden in the malpighian tubules.

4.2.1   Bisphosphonate Based Fluorescent Probes

To assess the specificity of our bisphosphonate based fluorescent probes to hydroxyapatite and calcium containing stones, we subjected synthetic hydroxyapatite particles and pulverized samples of infrared spectroscopy confirmed human calcium oxalate stones to bright field, polarized light and fluorescent microscopy.

Alendronate-FITC strongly bound to synthetic hydroxy apatite particles and human calcium oxalate stone material, while our negative control did not show any binding. This study validates the use of Alendronate-FITC for *ex vivo* and *in vivo* imaging.

4.2.2   *Ex vivo* Imaging of *Drosophila* Malpighian Tubules

This study aimed to visualize and quantify calcium oxalate stone burden using the two lithogenic agent's sodium oxalate and ethylene glycol at concentrations of 0.05%, 0.1%, 0.5% and 1% *w/v*. Our results show that sodium oxalate is the more reliable lithogenic agent as compared to ethylene glycol which produces scanty and haphazard stones throughout the malpighian tubules. Sodium oxalate at concentrations of 0.1% and 0.5% *w/v* produced stones in the main segments of the malpighian tubules. These

concentrations were used for our subsequent drug screening experiments. A concentration of 1% *w/v* sodium oxalate produced the highest number of stones and was used for our scanning electron microscopy and energy dispersive x-ray spectroscopy analysis.

4.2.3   *In vivo* Imaging of *Drosophila* Malpighian Tubules

To our knowledge this is the first report of intravital confocal imaging of *Drosophila* malpighian tubules. This section of our study develops a unique protocol for imaging *Drosophila* malpighian tubules *in vivo* using a transgenic red fluorescent protein expressing fly. We were successful in imaging malpighian tubules in both live larvae and adult flies. This platform will serve as a starting point for intravital imaging in the *Drosophila* model of nephrolithiasis and provide real-time information on the sites where crystallization begins plus help in monitoring stone burden to the assess the effects of therapeutic interventions.

4.3   Elemental Analysis of *Drosophila* Stones

We extracted and isolated stones formed by *Drosophila* for use in scanning electron microscopy and energy dispersive x-ray spectroscopy analysis to ascertain their elemental composition. For our model to be truly translatable to human nephrolithiasis, the stones formed should be similar in composition to their human counterparts.

The protocol that we developed for stone extraction and isolation was successful and provided an adequate sample yield. *Proteinase K* based malpighian tubule dissolution did not adversely affect the formed calcium oxalate stones. It was noted that a minimum of

150 dissected flies were required for sufficient sample collection. In some cases, light sonication for 30 minutes helped dislodge the stones from the malpighian tubules.

SEM analysis revealed that in the presence of the lithogenic agent's sodium oxalate and ethylene glycol, *Drosophila* formed predominately calcium oxalate stones. Both of the monohydrate and dihydrate forms of calcium oxalate were observed. Scanning electron microscopy analysis demonstrated pathognomonic dumbbell shaped calcium oxalate monohydrate crystals and envelope shaped calcium oxalate dihydrate crystals. Crystal size ranged between 6 to 16 μm which is roughly equal to the size of the malpighian tubule lumen and similar to the size of crystals formed in rat models of nephrolithiasis[98].

Energy dispersive x-ray spectroscopy analysis showed peaks of calcium (9.2% ± 1.33), carbon (35.1% ± 7.74) and oxygen (55.5% ± 6.71) which confirms that the crystal composition is predominantly calcium oxalate $(Ca(COO)_2)$. Carbon and oxygen was found in ratios of 1:1 and 1:2 which corroborates the di-anionic structure of oxalate. Trace amounts of magnesium were also observed in the calcium oxalate stones which is similar to that found in human stones. Our SEM/EDX analysis proves that the calcium oxalate stones formed in *Drosophila* closely resemble human calcium oxalate nephrolithiasis[134].

4.4   High-throughput Drug Screening Platform

As highlighted in the introduction to this project, kidney stone disease continues to be a significant healthcare issue and accounts for a large portion of urological practice. The advent of minimally invasive surgical techniques such as ureteroscopy (URS),

extracorporeal shockwave lithotripsy (ESWL), and percutaneous nephrolithotomy (PCNL) have led to improved clinical outcomes in patients with kidney stone disease, however, advancements in the medical management of kidney stones are severely lacking. Current medical therapies focus on prevention of kidney stones through dietary modification, such as increased fluid intake whilst limiting the intake of animal protein, dietary oxalate and sodium. Few, if any, drugs exist that directly target stone formation. Current therapies involve the use of thiazide diuretics such as hydrochlorothiazide and chlorthalidone, that act by inducing minor volume depletion leading to the reabsorption of sodium and concomitant passive reabsorption of filtered calcium[136,137]. A reduction in urinary calcium leads to a decreased risk of calcium oxalate stone formation. However, the use of thiazide diuretics is a preventative measure and does not affect stones that have already formed. Potassium citrate, a potent citrate source, is commonly prescribed as citrate forms complexes with enteric calcium and prevents it from binding to oxalate[138]. Potassium citrate can also quickly metabolize to bicarbonate and is used to alkalinize the urine in patients with uric acid stone disease. *Xanthine oxidase* inhibitors such as Allopurinol are used to reduce uric acid production and are useful in both patients with uric acid and calcium oxalate stone disease[139–141]. A need exists for improved medical management of kidney stone disease.

This section of our study utilizes the novel *Drosophila melanogaster* model of human calcium oxalate nephrolithiasis to screen through a library of 360 nutraceutical compounds to identify drugs that inhibit stone formation. The rationale for using this drug library stems from the proven association between the diet and kidney stone disease. Furthermore, nutraceuticals have been an effective starting point for rational drug design

in the past[130]. For example, Faber *et. al.* in their landmark paper discovered that

administration of folic acid in children with acute lymphoblastic leukemia (ALL) caused

an exacerbation of the disease process which ultimately led to the development of the

now commonly used anti-metabolite chemotherapeutic agents[142]. Similar drug libraries

have recently been used to identify novel chemotherapeutic drugs[133].

As with prior animal models, no method existed for large scale drug screening in the

Drosophila model of human kidney stone disease. Our novel indirect screening method

for measuring stone burden in fly fecal matter was highly effective. Large cohorts of

drugs were easily screened in weeks using simple polarized and confocal microscopy.

The experimental protocol proved simple, was easily learned and did not require an

extensive infrastructure.

A total of 6 compounds that reduced calcium oxalate stone formation were identified for

a total of 360 compounds. A brief literature search revealed interesting information

regarding the possible mechanisms by which these drugs may have exerted their effect.

Aloin B is an anthrone derived from the leaves of the plant *Aloe trichosantha*. It is a

potent chloride channel activator that initiates peristalsis in human tissues such as the gut

and kidneys. Peristaltic action could potentially lead to early clearance of smaller calcium

oxalate crystals limiting their ability to form larger stones. Aloin B is a known

antimicrobial with a broad spectrum of action[143]. Since kidney stones are associated with

urinary tract infections, the action of Aloin B on the renal microbiome could reduce the

risk of stone formation. Additionally, Aloin B is also an antioxidant with anti-

inflammatory properties, as shown in prior studies[144]. Neutralization of reactive oxygen

species in the urinary tract and reduction of the inflammation associated with the deposition of calcium oxalate crystals could also reduce the risk of stone formation.

Alpha Mangostin is a xanthoid that is isolated from the mangosteen tree. Previous studies on its pharmacological activity have shown potent anti-oxidant, anti-microbial and anti-inflammatory properties[145,146]. Similarly, mangostin is basic in nature and could potentially alkalinize the urine leading to effects similar to that of potassium citrate.

Cucurbatacin B is compound that imparts a bitter taste to plant species in the *Cucurbitaceae* family which includes squashes and pumpkins. It has known anti-cancer properties as shown in a number of studies[147,148].

Arbutin is a glycoside that inhibits *tyrosinase* and is extracted from the leaf of the bearberry plant. It has previously been used in traditional Cherokee medicine as a urinary tract infection remedy and recent studies have validated its antimicrobial effect[149].

Isorhamnetin is a methylated flavonoid that is isolated from the psychedelic plant *Tagetes lucida*. Isorhamnetin has known anti-mycobacterial and anti-inflammatory properties plus stabilizing effects on the renal cell membrane[150–152]. There is some evidence of the potential action of Isorhamnetin on Vitamin D receptor (VDR) activation that might cause changes in calcium metabolism leading to a decreased risk of calcium oxalate stone formation[153].

Apiin is an aglycone isolated from parsley and celery. It and other apigenins have been previously used for treatment of urinary tract infections and urolithiasis[154]. It acts by

exerting a diuretic action through the inhibition of the $Na^+K^+ATPase$ pump in renal tissues[155].

Our drug screening platform has yielded some interesting results. Further investigation of the possible mechanisms of action of these drugs will be required to validate these results.

4.5   Future Directions

Future work in this area will aim to elucidate the mechanisms of action of these drugs. We also wish to screen larger libraries of FDA approved drugs to further strengthen our results. Additionally, we have developed and optimized protocols for *in vivo* imaging of *Drosophila* nephrolithiasis. Our next step will be to use our novel bisphosphonate based fluorescent probes to visualize stone formation in real time. This will provide us with vital information on where and how crystallization begins, possibly exposing new therapeutic targets.

Most nephrolithiasis research is targeted towards the prevention and treatment of calcium oxalate stones which is the most common subtype. We also aim to develop additional *Drosophila* models for other stone types such as cystine and uric acid. Work is currently underway to develop a simple genetic *Drosophila* model for cystine nephrolithiasis. We have identified 16 DM orthologues for the human cystine co-transporters *SLC3A1* and *SLC7A9* using the *Drosophila* RNAi Orthologue Online Prediction Tool **(Figure 28)**. Of the 16 gene orthologs identified, fly gene CG9413 is an exact match for structure and function in the fly renal tubules. Using this data, we have created a transgenic fly that

possesses the *SLC7A9* gene knockdown in the principal cells of the malpighian tubules

by utilizing GAL4/UAS system. Two fly lines were obtained, one expressing the yeast

transcription activation factor (GAL4) in its renal tubules and a second fly line in which

an upstream activation sequence (UAS) is followed by a hairpin dsRNA sequence

directed against gene CG9413. The mating of these lines resulted in a selective

knockdown of the cystine co-transporter in the principal cells of the malpighian tubule.

Search Term	Human Gene ID	HGNC	Human Symbol	Fly Gene ID	FlyBase	Fly Symbol	Score	Weighted Score	Prediction Derived From	Alignment & Scores
SLC7A9	11136	11067	SLC7A9	32397	FBgn0030574	CG9413	10	9.669	Compara, Homologene, Inparanoid, Isobase, OMA, OrthoDB, orthoMCL, Phylome, RoundUp, TreeFam	View
SLC7A9	11136	11067	SLC7A9	34624	FBgn0028425	Jhl-21	4	3.854	Isobase, OrthoDB, orthoMCL, RoundUp	View
SLC7A9	11136	11067	SLC7A9	43707	FBgn0039844	CG1607	3	2.904	OrthoDB, orthoMCL, RoundUp	View
SLC7A9	11136	11067	SLC7A9	39625	FBgn0002778	mnd	3	2.904	OrthoDB, orthoMCL, RoundUp	View
SLC7A9	11136	11067	SLC7A9	43265	FBgn0039487	gb	3	2.851	Isobase, OrthoDB, orthoMCL	View
SLC7A9	11136	11067	SLC7A9	32986	FBgn0031064	CG12531	1	1.003	RoundUp	View
SLC3A1	6519	11025	SLC3A1	35828	FBgn0050359	Mal-A5	7	6.708	Compara, Inparanoid, Isobase, OMA, orthoMCL, Phylome, RoundUp	View
SLC3A1	6519	11025	SLC3A1	34598	FBgn0032382	Mal-B2	6	5.803	Compara, Homologene, Isobase, OMA, Phylome, RoundUp	View
SLC3A1	6519	11025	SLC3A1	35830	FBgn0033297	Mal-A8	6	5.705	Compara, Inparanoid, Isobase, OMA, orthoMCL, Phylome	View
SLC3A1	6519	11025	SLC3A1	35827	FBgn0033294	Mal-A4	6	5.698	Compara, Inparanoid, Isobase, orthoMCL, Phylome, RoundUp	View
SLC3A1	6519	11025	SLC3A1	34597	FBgn0032381	Mal-B1	6	5.695	Compara, Homologene, Inparanoid, Isobase, orthoMCL, Phylome	View
SLC3A1	6519	11025	SLC3A1	35825	FBgn0002569	Mal-A2	5	4.755	Compara, Inparanoid, OMA, orthoMCL, Phylome	View
SLC3A1	6519	11025	SLC3A1	246565	FBgn0050360	Mal-A6	5	4.755	Compara, Inparanoid, OMA, orthoMCL, Phylome	View
SLC3A1	6519	11025	SLC3A1	35826	FBgn0002571	Mal-A3	5	4.755	Compara, Inparanoid, OMA, orthoMCL, Phylome	View
SLC3A1	6519	11025	SLC3A1	35829	FBgn0033296	Mal-A7	5	4.748	Compara, Inparanoid, orthoMCL, Phylome, RoundUp	View
SLC3A1	6519	11025	SLC3A1	35824	FBgn0002570	Mal-A1	5	4.695	Compara, Inparanoid, Isobase, orthoMCL, Phylome	View

Figure 28: Results of the DIOPT-DIST database search for *Drosophila* orthologs of human SLC7A9 and SLC3A9 genes.

Initial results are promising. Highly birefringent crystals were observed the throughout

the malpighian tubule and gut in transgenic *SLC7A9* knockdown *Drosophila* fed a 1%

cystine diet **(Figure 29)**. Similar crystals were not seen in the control wild type Canton-S

group.
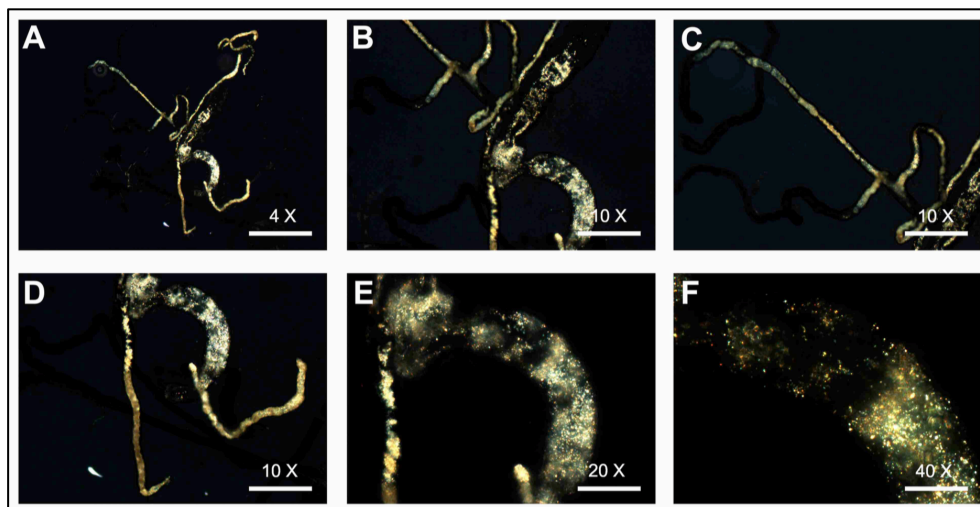
Figure 29: Polarized light microscopy of malpighian tubules from transgenic SLC7A9 knockdown *Drosophila* fed a 1% cystine diet.

Scanning electron microscopy and energy dispersive x-ray spectroscopy analysis of stones isolated from transgenic *SLC7A9* knockdown *Drosophila* revealed large (> 100 μm) heterogeneous stones **(Figure 30)**.

The stones were mostly composed of calcium and phosphate, however, there was a large organic component. Further analysis of these stones with high performance liquid chromatography – mass spectroscopy (HPLC-MS) is planned in the future.
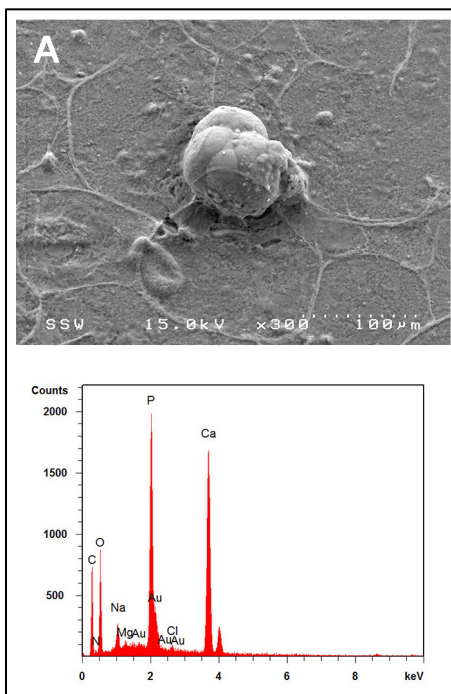
Figure 30: Scanning electron micrograph and energy dispersive x-ray diffraction spectroscopy analysis of stones isolated from the transgenic SLC7A9 knockdown Drosophila.

Similarly, we are also working on a *Drosophila* model for uric acid nephrolithiasis. Uric acid, which is a byproduct of purine metabolism in humans, is converted to allantoin via the action of the enzyme *Uricase* in invertebrates such as *Drosophila*. We have developed a transgenic *Uricase* knockdown fly that produces uric acid concretions when fed a diet high in purines **(Figure 31)**.

Figure 31: Polarized light microscopy of malpighian tubules from transgenic *Uricase* knockdown *Drosophila* fed (A) standard food media (B) high yeast media (C) 1% purine media.

SEM/EDX analysis of stones isolated from transgenic *Uricase* knockdown *Drosophila* show a composition similar to that of human uric acid stones **(Figure 32)**.
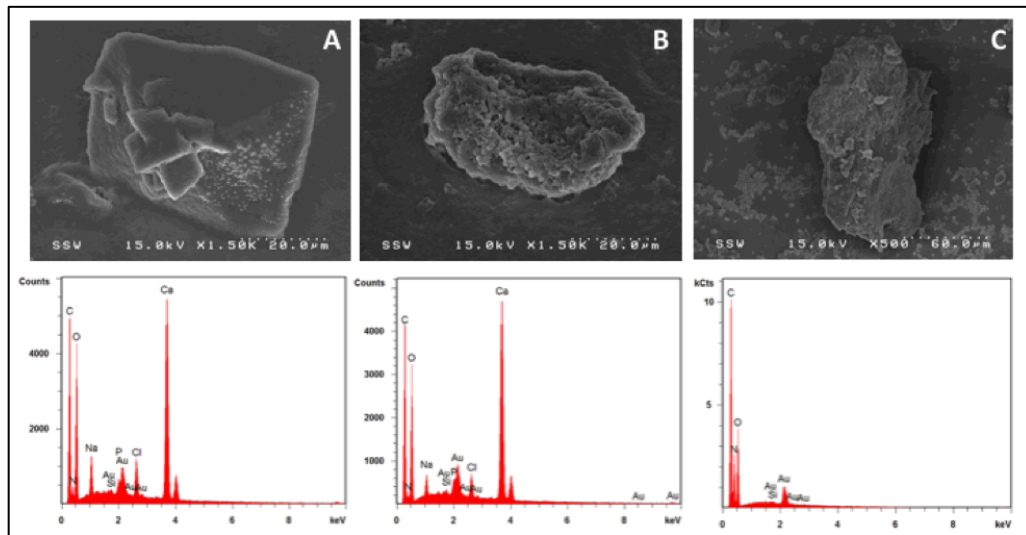
Figure 32: SEM/EDX analysis of stones isolated from transgenic *Uricase* knockdown *Drosophila*. (A,B) *Drosophila* stone sample (C) Control human uric acid stone sample.

Future experiments are planned to develop *Drosophila* models for other stone types such as struvite, and screen large libraries of FDA approved drugs to identify potential therapies. Work is also being done to investigate the effects of gut and urinary microbiome on stone formation. We are confident that work in this novel model will impact patient care and benefit patients with nephrolithiasis in a dramatic way.

Bibliography

1.   Scales CD, Smith AC, Hanley JM, et al: Prevalence of kidney stones in the United States. Eur. Urol. 2012; **62**: 160–165.

2.   Stamatelou KK, Francis ME, Jones C a., et al: Time trends in reported prevalence of kidney stones in the United States: 1976-1994. Kidney Int. 2003; **63**: 1817–1823.

3.   Lotan Y, Cadeddu J a, Roerhborn CG, et al: Cost-effectiveness of medical management strategies for nephrolithiasis. J. Urol. 2004; **172**: 2275–2281.

4.   Clark JY, Thompson IM and Optenberg SA: Economic impact of urolithiasis in the United States. J. Urol. 1995; **154**: 2020–4.

5.   Saigal CS, Joyce G and Timilsina AR: Direct and indirect costs of nephrolithiasis in an employed population: Opportunity for disease management? Kidney Int. 2005; **68**: 1808–1814.

6.   Coe FL, Parks JH and Asplin JR: The pathogenesis and treatment of kidney stones. N. Engl. J. Med. 1992; **327**: 1141–52.

7.   Sakhaee K, Maalouf NM and Sinnott B: Clinical review. Kidney stones 2012: pathogenesis, diagnosis, and management. J. Clin. Endocrinol. Metab. 2012; **97**: 1847–60.

8.   Millman S, Strauss AL, Parks JH, et al: Pathogenesis and clinical course of mixed calcium oxalate and uric acid nephrolithiasis. Kidney Int. 1982; **22**: 366–70.

9.   Denstedt JD and Fuller A: Urolithiasis. (Edited by JJ Talati, H-G Tiselius, DM Albala, et al). London: Springer London; 2012.

10.   Fattah Hasan, Hambaroush Yasmin GD: Cystine Nephrolithiasis. Transl Androl Urol 2014; **3**: 228–233.

11.   Pais VM, Lowe G, Lallas CD, et al: Xanthine urolithiasis. Urology 2006; **67**: 1084.e9–1084.e11.

12.   Ramello A, Vitale C and Marangella M: Epidemiology of nephrolithiasis. J. Nephrol. 2000; **13 Suppl 3**: S45–50.

13.   Pak CYC, Poindexter JR, Adams-Huet B, et al: Predictive value of kidney stone composition in the detection of metabolic abnormalities. Am. J. Med. 2003; **115**: 26–32.

14.   Chen YY, Roseman JM, Devivo MJ, et al: Geographic variation and environmental risk factors for the incidence of initial kidney stones in patients with spinal cord injury. J. Urol. 2000; **164**: 21–6.

15.   Brikowski TH, Lotan Y and Pearle MS: Climate-related increase in the prevalence of urolithiasis in the United States. Proc. Natl. Acad. Sci. U. S. A. 2008; **105**: 9841–6.

16.   Pak CY: Etiology and treatment of urolithiasis. Am. J. Kidney Dis. 1991; **18**: 624–

37.

17. Frick KK and Bushinsky DA: Molecular mechanisms of primary hypercalciuria. J. Am. Soc. Nephrol. 2003; **14**: 1082–95.

18. Pak CY, Britton F, Peterson R, et al: Ambulatory evaluation of nephrolithiasis. Classification, clinical presentation and diagnostic criteria. Am. J. Med. 1980; **69**: 19–30.

19. Curhan GC and Taylor EN: 24-h uric acid excretion and the risk of kidney stones. Kidney Int. 2008; **73**: 489–96.

20. Broadus AE, Insogna KL, Lang R, et al: A consideration of the hormonal basis and phosphate leak hypothesis of absorptive hypercalciuria. J. Clin. Endocrinol. Metab. 1984; **58**: 161–9.

21. Insogna KL, Broadus AE, Dreyer BE, et al: Elevated production rate of 1,25-dihydroxyvitamin D in patients with absorptive hypercalciuria. J. Clin. Endocrinol. Metab. 1985; **61**: 490–5.

22. Sorensen MD, Eisner BH, Stone KL, et al: Impact of calcium intake and intestinal calcium absorption on kidney stones in older women: the study of osteoporotic fractures. J. Urol. 2012; **187**: 1287–92.

23. Li XQ, Tembe V, Horwitz GM, et al: Increased intestinal vitamin D receptor in genetic hypercalciuric rats. A cause of intestinal calcium hyperabsorption. J. Clin. Invest. 1993; **91**: 661–7.

24. Karnauskas AJ, van Leeuwen JPTM, van den Bemd G-JCM, et al: Mechanism and function of high vitamin D receptor levels in genetic hypercalciuric stone-forming rats. J. Bone Miner. Res. 2005; **20**: 447–54.

25. Coe FL and Bushinsky DA: Pathophysiology of hypercalciuria. Am. J. Physiol. 1984; **247**: F1–13.

26. Buckalew VM: Nephrolithiasis in renal tubular acidosis. J. Urol. 1989; **141**: 731–7.

27. Patron P, Gardin JP and Paillard M: Renal mass and reserve of vitamin D: determinants in primary hyperparathyroidism. Kidney Int. 1987; **31**: 1174–80.

28. Lau YK, Wasserstein A, Westby GR, et al: Proximal tubular defects in idiopathic hypercalciuria: resistance to phosphate administration. Miner. Electrolyte Metab. 1982; **7**: 237–49.

29. Levi M and Breusegem S: Renal Phosphate–Transporter Regulatory Proteins and Nephrolithiasis. N. Engl. J. Med. 2008; **359**: 1171–1173.

30. Karim Z, Gérard B, Bakouh N, et al: NHERF1 Mutations and Responsiveness of Renal Parathyroid Hormone. N. Engl. J. Med. 2008; **359**: 1128–1135.

31. Sakhaee K: Recent advances in the pathophysiology of nephrolithiasis. Kidney Int. 2009; **75**: 585–595.

32. Smith LH: Diet and hyperoxaluria in the syndrome of idiopathic calcium oxalate urolithiasis. Am. J. Kidney Dis. 1991; **17**: 370–5.

33. Watts RW: Primary hyperoxaluria type I. QJM 1994; **87**: 593–600.

34. Danpure CJ: Molecular and clinical heterogeneity in primary hyperoxaluria type 1. Am. J. Kidney Dis. 1991; **17**: 366–9.

35. Hoppe B: An update on primary hyperoxaluria. Nat. Rev. Nephrol. 2012; **8**: 467–475.

36. Parks JH, Worcester EM, O'Connor RC, et al: Urine stone risk factors in nephrolithiasis patients with and without bowel disease. Kidney Int. 2003; **63**: 255–65.

37. McConnell N, Campbell S, Gillanders I, et al: Risk factors for developing renal stones in inflammatory bowel disease. BJU Int. 2002; **89**: 835–41.

38. Annuk M, Backman U, Holmgren K, et al: Urinary calculi and jejunoileal bypass operation. A long-term follow-up. Scand. J. Urol. Nephrol. 1998; **32**: 177–80.

39. Dobbins JW and Binder HJ: Effect of bile salts and fatty acids on the colonic absorption of oxalate. Gastroenterology 1976; **70**: 1096–1100.

40. Lindsjö M, Danielson BG, Fellström B, et al: Intestinal oxalate and calcium absorption in recurrent renal stone formers and healthy subjects. Scand. J. Urol. Nephrol. 1989; **23**: 55–9.

41. Sidhu H, Hoppe B, Hesse A, et al: Absence of Oxalobacter formigenes in cystic fibrosis patients: a risk factor for hyperoxaluria. Lancet 1998; **352**: 1026–1029.

42. Mittal RD, Kumar R, Mittal B, et al: Stone composition, metabolic profile and the presence of the gut-inhabiting bacterium Oxalobacter formigenes as risk factors for renal stone formation. Med. Princ. Pract. 2013; **12**: 208–13.

43. Duncan SH, Richardson AJ, Kaul P, et al: Oxalobacter formigenes and Its Potential Role in Human Health. Society 2002; **68**: 3841–3847.

44. Siva S, Barrack ER, Reddy GPV, et al: A critical analysis of the role of gut Oxalobacter formigenes in oxalate stone disease. BJU Int. 2009; **103**: 18–21.

45. Preminger GM: Renal calculi: pathogenesis, diagnosis, and medical therapy. Semin. Nephrol. 1992; **12**: 200–16.

46. Hess B, Zipperle L and Jaeger P: Citrate and calcium effects on Tamm-Horsfall glycoprotein as a modifier of calcium oxalate crystal aggregation. Am. J. Physiol. 1993; **265**: F784–91.

47. Asplin JR, Arsenault D, Parks JH, et al: Contribution of human uropontin to inhibition of calcium oxalate crystallization. Kidney Int. 1998; **53**: 194–199.

48. Pak CY: Citrate and renal calculi: an update. Miner. Electrolyte Metab. 1994; **20**: 371–7.

49. Kok DJ, Papapoulos SE and Bijvoet OL: Crystal agglomeration is a major element in calcium oxalate urinary stone formation. Kidney Int. 1990; **37**: 51–6.

50. Breslau NA, Brinkley L, Hill KD, et al: Relationship of animal protein-rich diet to kidney stone formation and calcium metabolism. J. Clin. Endocrinol. Metab. 1988;

66: 140–6.

51.   Mandel EI, Taylor EN and Curhan GC: Dietary and lifestyle factors and medical conditions associated with urinary citrate excretion. Clin. J. Am. Soc. Nephrol. 2013; **8**: 901–8.

52.   Borghi L, Meschi T, Amato F, et al: Urinary volume, water and recurrences in idiopathic calcium nephrolithiasis: a 5-year randomized prospective study. J. Urol. 1996; **155**: 839–43.

53.   Ferraro PM, Taylor EN, Gambaro G, et al: Soda and other beverages and the risk of kidney stones. Clin. J. Am. Soc. Nephrol. 2013; **8**: 1389–95.

54.   Curhan GC, Willett WC, Rimm EB, et al: Prospective study of beverage use and the risk of kidney stones. Am. J. Epidemiol. 1996; **143**: 240–7.

55.   Curhan GC, Willett WC, Speizer FE, et al: Beverage use and risk for kidney stones in women. Ann. Intern. Med. 1998; **128**: 534–40.

56.   Hönow R, Laube N, Schneider A, et al: Influence of grapefruit-, orange- and apple-juice consumption on urinary variables and risk of crystallization. Br. J. Nutr. 2003; **90**: 295–300.

57.   Muldowney FP, Freaney R and Moloney MF: Importance of dietary sodium in the hypercalciuria syndrome. Kidney Int. 1982; **22**: 292–6.

58.   Curhan GC, Willett WC, Speizer FE, et al: Comparison of dietary calcium with supplemental calcium and other nutrients as factors affecting the risk for kidney stones in women. Ann. Intern. Med. 1997; **126**: 497–504.

59.   Curhan GC, Willett WC, Knight EL, et al: Dietary factors and the risk of incident kidney stones in younger women: Nurses' Health Study II. Arch. Intern. Med. 2004; **164**: 885–91.

60.   Coe FL: Uric acid and calcium oxalate nephrolithiasis. Kidney Int. 1983; **24**: 392–403.

61.   Coe FL, Strauss AL, Tembe V, et al: Uric acid saturation in calcium nephrolithiasis. Kidney Int. 1980; **17**: 662–8.

62.   Coe FL and Parks JH: Hyperuricosuria and calcium nephrolithiasis. Urol. Clin. North Am. 1981; **8**: 227–44.

63.   Halabe A and Sperling O: Uric acid nephrolithiasis. Miner. Electrolyte Metab. 1994; **20**: 424–31.

64.   Maalouf NM, Sakhaee K, Parks JH, et al: Association of urinary pH with body weight in nephrolithiasis. Kidney Int. 2004; **65**: 1422–5.

65.   Taylor EN and Curhan GC: Body size and 24-hour urine composition. Am. J. Kidney Dis. 2006; **48**: 905–15.

66.   Coe FL: Hyperuricosuric calcium oxalate nephrolithiasis. Adv. Exp. Med. Biol. 1980; **128**: 439–50.

67.   Yu TF: Urolithiasis in hyperuricemia and gout. J. Urol. 1981; **126**: 424–30.

68. Kramer HM and Curhan G: The association between gout and nephrolithiasis: the National Health and Nutrition Examination Survey III, 1988-1994. Am. J. Kidney Dis. 2002; **40**: 37–42.

69. Griffith DP: Struvite stones. Kidney Int. 1978; **13**: 372–82.

70. Flannigan R, Choy WH, Chew B, et al: Renal struvite stones--pathogenesis, microbiology, and management strategies. Nat. Rev. Urol. 2014; **11**: 333–41.

71. Broomfield RJ, Morgan SD, Khan A, et al: Crystalline bacterial biofilm formation on urinary catheters by urease-producing urinary tract pathogens: a simple method of control. J. Med. Microbiol. 2009; **58**: 1367–1375.

72. Kristensen C, Parks JH, Lindheimer M, et al: Reduced glomerular filtration rate and hypercalciuria in primary struvite nephrolithiasis. Kidney Int. 1987; **32**: 749–53.

73. Kaefer M, Hendren WH, Bauer SB, et al: Reservoir calculi: a comparison of reservoirs constructed from stomach and other enteric segments. J. Urol. 1998; **160**: 2187–90.

74. Feliubadaló L, Font M, Purroy J, et al: Non-type I cystinuria caused by mutations in SLC7A9, encoding a subunit (bo,+AT) of rBAT. Nat. Genet. 1999; **23**: 52–7.

75. Mattoo A and Goldfarb DS: Cystinuria. Semin. Nephrol. 2008; **28**: 181–191.

76. Biyani CS and Cartledge JJ: Cystinuria-Diagnosis and Management. EAU-EBU Updat. Ser. 2006; **4**: 175–183.

77. Viprakasit DP, Sawyer MD, Herrell SD, et al: Changing composition of staghorn calculi. J. Urol. 2011; **186**: 2285–90.

78. Ichida K, Matsumura T, Sakuma R, et al: Mutation of human molybdenum cofactor sulfurase gene is responsible for classical xanthinuria type II. Biochem. Biophys. Res. Commun. 2001; **282**: 1194–200.

79. Perazella M a: Drug-Induced Renal Failure: Update on New Medications and Unique Mechanisms of Nephrotoxicity. Am. J. Med. Sci. 2003; **325**: 349–362.

80. Glowacki LS, Beecroft ML, Cook RJ, et al: The natural history of asymptomatic urolithiasis. J. Urol. 1992; **147**: 319–21.

81. Teichman JMH: Clinical practice. Acute renal colic from ureteral calculus. N. Engl. J. Med. 2004; **350**: 684–693.

82. KOBAYASHI T, NISHIZAWA K, MITSUMORI K, et al: Impact of Date of Onset on the Absence of Hematuria in Patients with Acute Renal Colic. J. Urol. 2003; **170**: 1093–1096.

83. Press SM and Smith AD: Incidence of negative hematuria in patients with acute urinary lithiasis presenting to the emergency room with flank pain. Urology 1995; **45**: 753–757.

84. Bove P, Kaplan D, Dalrymple N, et al: Reexamining the value of hematuria testing in patients with acute flank pain. J. Urol. 1999; **162**: 685–7.

85.   Tavichakorntrakool R, Prasongwattana V, Sungkeeree S, et al: Extensive characterizations of bacteria isolated from catheterized urine and stone matrices in patients with nephrolithiasis. Nephrol. Dial. Transplant. 2012; **27**: 4125–4130.

86.   Khan SR and Hackett RL: Calcium oxalate urolithiasis in the rat: is it a model for human stone disease? A review of recent literature. Scan. Electron Microsc. 1985: 759–74.

87.   Palma D, Langston C, Gisselman K, et al: Canine struvite urolithiasis. Compend. Contin. Educ. Vet. 2013; **35**: E1; quiz E1.

88.   Mandel NS, Henderson JD, Hung LY, et al: A porcine model of calcium oxalate kidney stone disease. J. Urol. 2004; **171**: 1301–3.

89.   Rosenow EC: The production of urinary calculi by the devitalization and infection of teeth in dogs with streptococci from cases of neprholithiasis. Arch. Intern. Med. 1923; **31**: 807.

90.   Bachmann S, Sakai T and Kriz W: Nephron and Collecting Duct Structure in the Kidney, Rat. In: 1986; pp 3–24.

91.   Khan SR and Hackett RL: Urolithogenesis of mixed foreign body stones. J. Urol. 1987; **138**: 1321–8.

92.   Khan SR, Glenton P a and Byer KJ: Modeling of hyperoxaluric calcium oxalate nephrolithiasis: experimental induction of hyperoxaluria by hydroxy-L-proline. Kidney Int. 2006; **70**: 914–23.

93.   de Water R, Boevé ER, van Miert PP, et al: Experimental nephrolithiasis in rats: the effect of ethylene glycol and vitamin D3 on the induction of renal calcium oxalate crystals. Scanning Microsc. 1996; **10**: 591–601; discussion 601–3.

94.   Oh SY, Kwon JK, Lee SY, et al: A comparative study of experimental rat models of renal calcium oxalate stone formation. J. Endourol. 2011; **25**: 1057–61.

95.   Khan SR and Glenton P a.: Experimental induction of calcium oxalate nephrolithiasis in mice. J. Urol. 2010; **184**: 1189–1196.

96.   Liu J, Cao Z, Zhang Z, et al: A comparative study on several models of experimental renal calcium oxalate stones formation in rats. J. Huazhong Univ. Sci. Technol. 2007; **27**: 83–87.

97.   Poldelski V, Johnson A, Wright S, et al: Ethylene glycol-mediated tubular injury: identification of critical metabolites and injury pathways. Am. J. Kidney Dis. 2001; **38**: 339–48.

98.   Khan SR: Animal models of kidney stone formation: an analysis. World J. Urol. 1997; **15**: 236–243.

99.   Lyon ES, Borden TA and Vermeulen CW: Experimental oxalate lithiasis produced with ethylene glycol. Invest. Urol. 1966; **4**: 143–51.

100.   Khan SR: Experimental calcium oxalate nephrolithiasis and the formation of human urinary stones. Scanning Microsc. 1995; **9**: 89–100; discussion 100–1.

101.   Khan SR: Calcium oxalate crystal interaction with renal tubular epithelium,

mechanism of crystal adhesion and its impact on stone development. Urol. Res. 1995; **23**: 71–9.

102.   Khan SR and Glenton PA: Deposition of calcium phosphate and calcium oxalate crystals in the kidneys. J. Urol. 1995; **153**: 811–7.

103.   Livrozet M, Vandermeersch S, Mesnard L, et al: An Animal Model of Type A Cystinuria Due to Spontaneous Mutation in 129S2/SvPasCrl Mice. Edited by D Long. PLoS One 2014; **9**: e102700.

104.   Miller J, Chi T, Kapahi P, et al: Drosophila melanogaster as an emerging translational model of human nephrolithiasis. J. Urol. 2013; **190**: 1648–56.

105.   Letsou A and Bohmann D: Small flies--big discoveries: nearly a century of Drosophila genetics and development. Dev. Dyn. 2005; **232**: 526–8.

106.   Pandey UB and Nichols CD: Human disease models in Drosophila melanogaster and the role of the fly in therapeutic drug discovery. Pharmacol. Rev. 2011; **63**: 411–36.

107.   Davies SA, Goodwin SF, Kelly DC, et al: Analysis and inactivation of vha55, the gene encoding the vacuolar ATPase B-subunit in Drosophila melanogaster reveals a larval lethal phenotype. J. Biol. Chem. 1996; **271**: 30677–84.

108.   Allan AK, Du J, Davies SA, et al: Genome-wide survey of V-ATPase genes in Drosophila reveals a conserved renal phenotype for lethal alleles. Physiol. Genomics 2005; **22**: 128–138.

109.   Karet FE, Finberg KE, Nelson RD, et al: Mutations in the gene encoding B1 subunit of H+-ATPase cause renal tubular acidosis with sensorineural deafness. Nat. Genet. 1999; **21**: 84–90.

110.   Hirata T, Cabrero P, Berkholz DS, et al: In vivo Drosophilia genetic model for calcium oxalate nephrolithiasis. Am. J. Physiol. Renal Physiol. 2012; **303**: F1555–62.

111.   Chien S, Reiter LT, Bier E, et al: Homophila: human disease gene cognates in Drosophila. Nucleic Acids Res. 2002; **30**: 149–51.

112.   Hu Y, Flockhart I, Vinayagam A, et al: An integrative approach to ortholog prediction for disease-focused and other functional studies. BMC Bioinformatics 2011; **12**: 357.

113.   Millburn GH, Crosby MA, Gramates LS, et al: FlyBase portals to human disease research using Drosophila models. Dis. Model. Mech. 2016; **9**: 245–52.

114.   Chintapalli VR, Wang J and Dow J a T: Using FlyAtlas to identify better Drosophila melanogaster models of human disease. Nat. Genet. 2007; **39**: 715–20.

115.   Duffy JB: GAL4 system in Drosophila: a fly geneticist's Swiss army knife. Genesis 2002; **34**: 1–15.

116.   Dietzl G, Chen D, Schnorrer F, et al: A genome-wide transgenic RNAi library for conditional gene inactivation in Drosophila. Nature 2007; **448**: 151–156.

117.   Weavers H, Prieto-Sánchez S, Grawe F, et al: The insect nephrocyte is a podocyte-

like cell with a filtration slit diaphragm. Nature 2009; **457**: 322–6.

118. Dow JA, Maddrell SH, Görtz A, et al: The malpighian tubules of Drosophila melanogaster: a novel phenotype for studies of fluid secretion and its control. J. Exp. Biol. 1994; **197**: 421–8.

119. Wessing A and Zierold K: The formation of type-I concretions in Drosophila Malpighian tubules studied by electron microscopy and X-ray microanalysis. J. Insect Physiol. 1999; **45**: 39–44.

120. Hirata T, Czapar A, Brin L, et al: Ion and solute transport by Prestin in Drosophila and Anopheles. J. Insect Physiol. 2012; **58**: 563–9.

121. Chen Y-H, Liu H, Chen H-Y, et al: Ethylene glycol induces calcium oxalate crystal deposition in Malpighian tubules: a Drosophila model for nephrolithiasis/urolithiasis. Kidney Int. 2011; **80**: 369–77.

122. Chen W-C, Lin W-Y, Chen H-Y, et al: Melamine-induced urolithiasis in a Drosophila model. J. Agric. Food Chem. 2012; **60**: 2753–7.

123. Chi T, Kim MS, Lang S, et al: A Drosophila model identifies a critical role for zinc in mineralization for kidney stone disease. PLoS One 2015; **10**: e0124150.

124. Lang S, Mutelifu G, Zee T, et al: OP2-05 A NOVEL GENETIC MODEL FOR STUDYING URIC ACID STONE DISEASE. J. Urol. 2014; **191**: e388–e389.

125. Ho C, Chen Y-H, Wu P, et al: Effects of commercial citrate-containing juices on urolithiasis in a Drosophila model. Kaohsiung J. Med. Sci. 2013; **29**: 488–493.

126. Tsai K-S, Chen Y-H, Shen J-L, et al: Does Chronic Cola Consumption Increase Urinary Stone Risk? Evidence from the <i>Drosophila</i> Model of Urolithiasis. J. Food Nutr. Res. 2015; **3**: 109–113.

127. Wu S-Y, Shen J-L, Man K-M, et al: An emerging translational model to screen potential medicinal plants for nephrolithiasis, an independent risk factor for chronic kidney disease. Evid. Based. Complement. Alternat. Med. 2014; **2014**: 972958.

128. Landry GM, Hirata T, Anderson JB, et al: Sulfate and thiosulfate inhibit oxalate transport via a dPrestin(mSlc26a6)-dependent mechanism in an insect model of calcium oxalate nephrolithiasis. Am. J. Physiol. Renal Physiol. 2015: ajprenal.00406.2015.

129. Gavin CT, Ali SN, Tailly T, et al: Novel Methods of Determining Urinary Calculi Composition: Petrographic Thin Sectioning of Calculi and Nanoscale Flow Cytometry Urinalysis. Sci. Rep. 2016; **6**: 19328.

130. Spagnuolo PA and Rogers MA: Food as a drug. Oncoscience 2015; **2**: 801–2.

131. Linford NJ, Bilgir C, Ro J, et al: Measurement of lifespan in Drosophila melanogaster. J. Vis. Exp. 2013: 1–9.

132. Cole LE, Vargo-Gogola T and Roeder RK: Bisphosphonate-functionalized gold nanoparticles for contrast-enhanced X-ray detection of breast microcalcifications. Biomaterials 2014; **35**: 2312–21.

133. Spagnuolo P: Interactions Between Nutraceutical Supplements and Standard Acute Myeloid Leukemia Chemotherapeutics. J. Pharm. Pharm. Sci. a Publ. Can. Soc. Pharm. Sci. Société Can. des Sci. Pharm. 2015; **18**: 339–43.

134. Ouyang J-M, Gao J, Xue J-F, et al: Nanouric acid or nanocalcium phosphate as central nidus to induce calcium oxalate stone formation: a high-resolution transmission electron microscopy study on urinary nanocrystallites. Int. J. Nanomedicine 2014; **9**: 4399.

135. Nazir A, Mukhopadhyay I, Saxena DK, et al: Evaluation of the No Observed Adverse Effect Level of Solvent Dimethyl Sulfoxide in Drosophila melanogaster. Toxicol. Mech. Methods 2003; **13**: 147–152.

136. Nijenhuis T, Vallon V, van der Kemp AWCM, et al: Enhanced passive Ca2+ reabsorption and reduced Mg2+ channel abundance explains thiazide-induced hypocalciuria and hypomagnesemia. J. Clin. Invest. 2005; **115**: 1651–8.

137. Nijenhuis T, Hoenderop JGJ, Loffing J, et al: Thiazide-induced hypocalciuria is accompanied by a decreased expression of Ca2+ transport proteins in kidney. Kidney Int. 2003; **64**: 555–564.

138. Fink HA, Wilt TJ, Eidman KE, et al: Medical Management to Prevent Recurrent Nephrolithiasis in Adults: A Systematic Review for an American College of Physicians Clinical Guideline. Ann. Intern. Med. 2013; **158**: 535.

139. Ettinger B, Tang A, Citron JT, et al: Randomized trial of allopurinol in the prevention of calcium oxalate calculi. N. Engl. J. Med. 1986; **315**: 1386–9.

140. Favus MJ and Coe FL: The effects of allopurinol treatment on stone formation on hyperuricosuric calcium oxalate stone-formers. Scand. J. Urol. Nephrol. Suppl. 1980; **53**: 265–71.

141. Kenny J-ES and Goldfarb DS: Update on the Pathophysiology and Management of Uric Acid Renal Stones. Curr. Rheumatol. Rep. 2010; **12**: 125–129.

142. Farber S, Diamond LK, Mercer RD, et al: Temporary Remissions in Acute Leukemia in Children Produced by Folic Acid Antagonist, 4-Aminopteroyl-Glutamic Acid (Aminopterin). N. Engl. J. Med. 1948; **238**: 787–793.

143. Oumer A, Bisrat D, Mazumder A, et al: A new antimicrobial anthrone from the leaf latex of Aloe trichosantha. Nat. Prod. Commun. 2014; **9**: 949–52.

144. Silva MA, Trevisan G, Hoffmeister C, et al: Anti-inflammatory and antioxidant effects of Aloe saponaria Haw in a model of UVB-induced paw sunburn in rats. J. Photochem. Photobiol. B Biol. 2014; **133**: 47–54.

145. Shankaranarayan D, Gopalakrishnan C and Kameswaran L: Pharmacological profile of mangostin and its derivatives. Arch. Int. Pharmacodyn. thérapie 1979; **239**: 257–69.

146. Jung H-A, Su B-N, Keller WJ, et al: Antioxidant Xanthones from the Pericarp of Garcinia mangostana (Mangosteen). J. Agric. Food Chem. 2006; **54**: 2077–2082.

147. Chen JC, Chiu MH, Nie RL, et al: Cucurbitacins and cucurbitane glycosides:

structures and biological activities. Nat. Prod. Rep. 2005; **22**: 386.

148. Kapoor S: Cucurbitacin B and its rapidly emerging role in the management of systemic malignancies besides lung carcinomas. Cancer Biother. Radiopharm. 2013; **28**: 359.

149. Dykes GA, Amarowicz R and Pegg RB: Enhancement of nisin antibacterial activity by a bearberry (Arctostaphylos uva-ursi) leaf extract. Food Microbiol. 2003; **20**: 211–216.

150. Jnawali HN, Jeon D, Jeong M-C, et al: Antituberculosis Activity of a Naturally Occurring Flavonoid, Isorhamnetin. J. Nat. Prod. 2016; **79**: 961–969.

151. Osman S, El Kashak W, Wink M, et al: New isorhamnetin derivatives from Salsola imbricata Forssk. leaves with distinct anti -inflammatory activity. Pharmacogn. Mag. 2016; **12**: 47.

152. Yokozawa T, Dong E, Kawai Y, et al: Protective effects of some flavonoids on the renal cellular membrane. Exp. Toxicol. Pathol. 1999; **51**: 9–14.

153. Inoue J, Choi J-M, Yoshidomi T, et al: Quercetin enhances VDR activity, leading to stimulation of its target gene expression in Caco-2 cells. J. Nutr. Sci. Vitaminol. (Tokyo). 2010; **56**: 326–30.

154. Farzaei MH, Abbasabadi Z, Ardekani MRS, et al: Parsley: a review of ethnopharmacology, phytochemistry and biological activities. J. Tradit. Chin. Med. 2013; **33**: 815–26.

155. Kreydiyyeh SI and Usta J: Diuretic effect and mechanism of action of parsley. J. Ethnopharmacol. 2002; **79**: 353–7.

Appendices

Appendix 1: Copyright Permission - The Journal Of Urology

Copyright
Clearance
Center

Confirmation Number: 11546026
Order Date: 03/09/2016

Customer Information

Customer: Sohrab Naushad Ali

This is not an invoice

Order Details

The journal of urology

		Billing Status: **N/A**	

Order detail ID:	69648604	**Permission Status:** ✅ Granted	
ISSN:	1527-3792	**Permission type:**	Republish or display content
Publication Type:	e-Journal	**Type of use:**	Thesis/Dissertation
Volume:		**Order License Id:**	3824910484988
Issue:			
Start page:		**Requestor type**	Academic institution
Publisher:	ELSEVIER INC	**Format**	Electronic
Author/Editor:	American Urological Association	**Portion**	chart/graph/table/figure
		Number of charts/graphs/tables/f igures	1
		Title or numeric reference of the portion(s)	Figure 1, Figure 3
		Title of the article or chapter the portion is from	Drosophila melanogaster as an Emerging Translational Model of Human Nephrolithiasis
		Editor of portion(s)	Elsevier
		Author of portion(s)	Joe Miller, Thomas Chi, Pankaj Kapahi, Arnold J. Kahn, Man Su Kim, Taku Hirata, Michael F. Romero, Julian A. T. Dow, Marshall L. Stoller
		Volume of serial or monograph	190
		Issue, if republishing an article from a serial	5
		Page range of portion	1648-56
		Publication date of portion	November 2013
		Rights for	Main product
		Duration of use	Life of current edition
		Creation of copies for the disabled	no
		With minor editing privileges	yes
		For distribution to	Canada
		In the following language(s)	Original language of publication
		With incidental promotional use	no
		Lifetime unit quantity of new product	Up to 499
		Made available in the following markets	Education, Thesis Repository
		The requesting person/organization	Sohrab Naushad Ali
		Order reference number	
		Author/Editor	Sohrab Naushad Ali
		The standard identifier	Thesis
		Title	The development of Novel Intravital Imaging and Drug Screen Platforms in the Drosophila Melanogaster Model for Human Calcium Oxalate Nephrolithiasis
		Publisher	University of Western Ontario
		Expected publication date	May 2016
		Estimated size (pages)	135

Note: This item was invoiced separately through our **RightsLink service.** More info $ 0.00

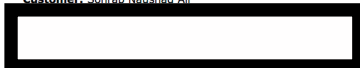|	
Total order items: 1	**Order Total: $0.00**

Appendix 2: Copyright Permission - Nature Publishing Group

Confirmation Number: 11546035
Order Date: 03/09/2016

Customer Information

Customer: Sohrab Naushad Ali

This is not an invoice

Order Details

Nature

			Billing Status: N/A

Order detail ID:	69648636	
ISSN:	1476-4687	
Publication Type:	e-Journal	
Volume:		
Issue:		
Start page:		
Publisher:	Nature Publishing Group	

Permission Status: ✓ Granted

Permission type:	Republish or display content
Type of use:	Republish in a thesis/dissertation
	Order License Id: 3824920092259
Requestor type	Academic institution
Format	Electronic
Portion	chart/graph/table/figure
Number of charts/graphs/tables/figures	1
Title or numeric reference of the portion(s)	Figure 1
Title of the article or chapter the portion is from	The insect nephrocyte is a podocyte-like cell with a filtration slit diaphragm
Editor of portion(s)	Nature Publishing Group
Author of portion(s)	Helen Weavers, Silvia Prieto-Sanchez, Ferdinand Grawe, Amparo Garcia-Lopez, Ruben Artero, Michaela Wilsch-Brauninger, Mar Ruiz-Gomez, Helen Skaer, Barry Denholm
Volume of serial or monograph	457
Issue, if republishing an article from a serial	7227
Page range of portion	322-6
Publication date of portion	January 2009
Rights for	Main product
Duration of use	Life of current edition
Creation of copies for the disabled	no
With minor editing privileges	yes
For distribution to	Canada
In the following language(s)	Original language of publication
With incidental promotional use	no
Lifetime unit quantity of new product	Up to 499
Made available in the following markets	Education, Thesis Repository
The requesting person/organization	Sohrab Naushad Ali
Order reference number	
Author/Editor	Sohrab Naushad Ali
The standard identifier	Thesis
Title	The development of Novel Intravital Imaging and Drug Screen Platforms in the Drosophila Melanogaster Model for Human Calcium Oxalate Nephrolithiasis
Publisher	University of Western Ontario
Expected publication date	May 2016
Estimated size (pages)	135

Note: This item was invoiced separately through our **RightsLink** service. More info   **$ 0.00**

Total order items: 1   **Order Total: $0.00**

Curriculum Vitae

Name:	Sohrab Naushad Ali

Post-secondary Education and Degrees:

Shifa College of Medicine
Islamabad, Pakistan
Jan 2005 – Dec 2009
M.B.B.S. Bachelor of Medicine, Bachelor of Surgery

Honours and Awards:

Western Graduate Research Scholarship (WGRS)
May 2015 – May 2016

Best Poster Presentation at the Robert Zhong Department of
Surgery Research Day
2015

Research Funding:

Schulich Masters in Surgery Research Grant $5,000
Principal Investigator
2015 – 2016

Lawson Health Research Institute Internal Research Grant $15,000
Co-Investigator
2015 – 2017

Related Work Experience

M.Sc. Candidate
Western University
London, Ontario, Canada
Lawson Health Research Institute
May 2015 – May 2016

Research Assistant
Western University
London, Ontario, Canada
Lawson Health Research Institute
Oct 2014 – May 2015

Research Assistant
Western University
London, Ontario, Canada
London Regional Cancer Program
Feb 2014 – May 2014

Resident Physician
Division of Urology
Northwest General Hospital
Peshawar, Pakistan
Mar 2012 – Feb 2013

Abstracts & Publications:

1.   **Sohrab Naushad Ali**, Jihye Kim, Paul Spagnuolo, Hassan Razvi, Hon Leong: High-Throughput and Non-Invasive Functional Drug Screening Platform for Drosophila Melanogaster Models of Nephrolithiasis. Abstract accepted at the Annual AUA Congress 2016.

2.   Kait Al, **Sohrab Naushad Ali**, Jihye Kim, Hon Leong, Hassan Razvi, Jeremy Burton: Characterization of the Microbiota Associated with Drosophila Models of Nephrolithiasis. Abstract accepted at the Annual AUA Congress 2016.

3.   Daniel Olvera-Posada, **Sohrab Naushad Ali**, Husain Alenezi, Marie Dion, John Denstedt, Hassan Razvi: Natural history of residual fragments after Percutaneous Nephrolithotomy (PCNL). Accepted for Podium Session at the Annual AUA Congress 2016.

4.   Carson Gavin, **Sohrab Naushad Ali**, Thomas Tailly, Daniel Olvera-Posada, Husain Alenezi, Nicholas Power, Jinqiang Hou, Andre St. Amant, Leonard Luyt, Stephen Wood, Charles Wu, Hassan Razvi, Hon Leong: Novel Methods of Determining Urinary Calculi Composition: Petrographic Thin Sectioning of Calculi and Nanoscale Flow Cytometry Urinalysis. Scientific Reports 5, 19328; doi:10.1038/srep19328 (2016). PMID: 26771074

5.   **Sohrab Naushad Ali**, Aymon Naushad Ali and Mian Naushad: Case Report Munchausen Syndrome by Proxy: The Overlooked Diagnosis. Journal of Ayub Medical College Abbottabad 2015; 27(2): 489–491. PMID: 26411148

6.   **Sohrab Naushad Ali**, Dajung Kim, Thomas Tailly, Hassan Razvi, Hon Leong: MP34-07 Intravital Imaging of the Drosophila Melanogaster Model of Human Nephrolithiasis. Journal of Urology 2015; 193(4): e412–e413. doi:10.1016/j.juro.2015.02.1303

7.   **Sohrab Naushad Ali**, Dajung Kim, Thomas Tailly, Hassan Razvi, Hon Leong: Fluorescent Imaging of the Drosophila Melanogaster Model of Human Nephrolithiasis. The 56th Annual Drosophila Conference GSA, Chicago USA 2015.

8.   **Sohrab Naushad Ali**, Niqad Ahmed, Aymon Naushad Ali, Mian Naushad: Emphysematous Pyelonephritis: A Review of Six Cases. Journal of Ayub Medical College Abbottabad 2014; 26(4): 591–597. PMID: 25672195

9.   **Sohrab Naushad Ali**, Aymon Naushad Ali, Niqad Ahmed, Mian Naushad: Ureteral triplication with vesicoureteral reflux and contralateral duplication. Journal of Ayub Medical College Abbottabad 2014; 24(5): 429–432. PMID: 25603691

Poster Presentations:

1.   **Sohrab Naushad Ali**, Dajung Kim, Thomas Tailly, Hassan Razvi, Hon Leong: Intravital Imaging of the Drosophila Melanogaster Model of Human Nephrolithiasis – Dr. Robert Zhong Department of Surgery Research Day, London, Ontario.

2.   **Sohrab Naushad Ali**, Dajung Kim, Thomas Tailly, Hassan Razvi, Hon Leong: MP34-07 Intravital Imaging of the Drosophila Melanogaster Model of Human Nephrolithiasis – Annual AUA Congress New Orleans.

3.   **Sohrab Naushad Ali**, Dajung Kim, Thomas Tailly, Hassan Razvi, Hon Leong: Fluorescent Imaging of the Drosophila Melanogaster Model of Human Nephrolithiasis – The 56th Annual Drosophila Conference GSA, Chicago.

Invited Lectures:

1.   JK Wyatt Urology Residents Research Day
        Double Tree Hilton, London, ON
        April 26th, 2016.

1.   Lawson Health Research Institute 'Talks on Friday'
        Shuttleworth Auditorium, St. Joseph's Hospital
        February 12th, 2016.

2.   Lawson Health Research Institute 'Talks on Friday'
        Shuttleworth Auditorium, St. Joseph's Hospital
        November 28th, 2014.